Doctoral Dissertation

Effect of Protic Molten Salt on Electrocatalytic Performance of Pt Nanoparticles Prepared by the Ionic Liquid-Sputtering Method

Reiko Izumi

July 2018

Department of Applied Chemistry

Graduate School of Engineering,

Osaka University

Effect of Protic Molten Salt on Electrocatalytic Performance of Pt Nanoparticles Prepared by the Ionic Liquid-Sputtering Method

（イオン液体ースパッタリング法で調製した Pt ナノ粒子の電極触媒能へ与えるプロトン性溶融塩の影響）

2018

Reiko Izumi

Department of Applied Chemistry

Graduate School of Engineering

Osaka University

Preface

The studies presented in this thesis were carried out under the guidance of Professor Dr. Susumu Kuwabata at Department of Applied Chemistry, Graduate School of Engineering, Osaka University during 2014-2018.

The object of this thesis is to develop the novel Pt nanoparticles-supported carbon catalyst using ionic liquid for oxygen reduction reaction to achieve high catalytic activity and durability. It involves exploring the undeveloped function of ionic liquid and molten salt. The author hopes sincerely that the findings obtained in the studies would contribute to progress science and technology in the field of ionic liquid or molten salt and fuel cell catalyst.

Reiko Izumi

Department of Applied Chemistry,

Graduate School of Engineering,

Osaka University

Suita, Osaka,

Japan

July, 2018

Contents

General Introduction

The fuel cell, which is a kind of energy conversion devices, generates electric energy from appropriate chemical fuels, such as hydrogen, alcohols, and hydrazine with higher conversion efficiencies than those for the respective burning reactions. In particular, the hydrogen-oxygen fuel cell, which emits water alone, has attracted much attention because of its high applicability to a clean energy source in place of the internal-combustion engine. The polymer electrolyte fuel cell (PEFC) that has several advantages including high power density, low-operating temperatures, high start-up performance, and compactness[1-5] is invented by BALLARD Inc. in 1994 in order to mount it in automobiles driven by electric motors. After years of development research done all over the world, Toyota Motor Company put a PEFC sedan, "Mirai", on the market in 2014.

However, the current fuel cells driven in ambient temperature possess inherent drawback that is a requirement of expensive Pt-based electrocatalysts for enhancing the cathodic oxygen reduction reaction (ORR) because the ORR at a positive electrode is considerably slow compared to electrochemical oxidation of fuels at a negative electrode.[1-5] In addition, there is a mortal drawback that is relatively low durability of Pt catalyst. The Pt catalyst is composed of Pt nanoparticles deposited on a carbon black grains, the latter of which serve electron and gas paths when an electrode is fabricated using the Pt catalysts with an appropriate binder material.[1-5] When a fuel cell is operated, the electrode potential of a positive electrode, on which the ORR occurs, becomes around 0.9 V vs. NHE. However, large change in load due to sudden acceleration and harsh braking sometimes makes the electrode potential shift to 1.0 V vs. NHE or higher that is positive enough to cause oxidative degradation of the carbon supporter.[6-13] Unfortunately Pt is also a good catalyst toward the degradation reactions such as conversion of carbon to carbon dioxide.[11-14] Consequently, Pt nanoparticles that lose their

supporter aggregate and disperse in water generated in the PEFC, resulting in performance loss.[6-14] In other words, the PEFC vehicles run while throwing away valuable Pt metal particles on the ground. Accordingly, it is a high-priority issue to develop ways to prevent the degradation of the carbon supporter for realizing the anticipated future market expansion. As aforementioned, the degradation reaction is catalyzed by Pt, implying that the Pt nanoparticles directly contacting to the carbon supporter work well. So far, several approaches have been proposed to improve the Pt catalyst durability[15-27], such as the use of sp^2-carbon materials (carbon nanotubes[15-17] and graphene[18-20]), SiO_2 coating on the carbon supports,[21] and non-carbon support materials.[22-24] Although these approaches have been effective in reducing the degradation in varying degrees, further developments would be required because of the high costs, complex preparation procedures, and insufficient electrode performances resulting from the those approaches. Hence, development of an effective means to provide high durability to the Pt catalysts with keeping their high catalytic activities is a challenging subject.

Room-temperature ionic liquids (IL) is a liquid salt consisting entirely of cations and anions at room temperature and is a subset of a molten salt. The unique features of IL, such as negligible vapor pressure, wide electrochemical window, good thermal stability, and antistatic properties, have led to many proposed applications thus far.[28-37] Among such features, the research group I belong to focused on the extremely low vapor pressure, which enables one to put the liquid even in vacuum condition. There are many kinds of instruments that require vacuum condition in their sample chambers. It is strictly forbidden to introduce any conventional molecular liquid into these vacuum equipments because of contamination due to liquid vaporization. Since the research group noticed that IL can be put in the vacuum chamber, they began to subject ILs to analysis and process with several vacuum instruments.[38-41]

One of the techniques they developed is a metal nanoparticles preparation method named "IL-sputtering method".[41-59] Because of IL's non-volatility, metal sputtering onto IL surface is possible under reduced pressure, giving metal nanoparticles suspended in the IL. In the case

of noble metal nanoparticles, stabilization effect by IL prevent aggregation of the nanoparticles for a long time.[41-43,60-64] When nanoparticles of metals that are susceptible to oxidation like copper and indium are prepared and the resulting metal nanoparticle-suspended IL is left in air, oxidation of the nanoparticles without aggregation, giving metal oxide nanoparticles dispersed in IL.[49,50] Sputtering onto IL using arrayed two kinds of metal as a target produces alloy nanoparticles.[44,47,53,54] By this way, Pt nanoparticles were prepared by Pt sputtering onto IL, and it was found that agitating the resulting IL with various carbon supports, e.g., carbon nanotubes and carbon black, under heating condition induced immobilization of Pt nanoparticles on the surfaces of the carbon materials. The prepared Pt nanoparticles deposited on the carbon (Pt/C) were found to exhibit favorable electrocatalytic activity toward ORR.[48,56,59] Notably the prepared Pt/C catalyst possessed higher durability than commercially available Pt/C catalyst when they were examined by the standard degradation test recommended by the Fuel Cell Commercialization Conference of Japan (FCCJ).[59] Based on several analyses of the sample, it was concluded that the thin IL layer existing as a paste between the Pt nanoparticles and carbon support prevented direct contact of Pt with carbon support and consequently suppressed the carbon support corrosion.[59] This is quite desirable feature but the presence of the insulating IL layer between the Pt nanoparticle and carbon support might retard charge transfer, resulting in the initial electrocatalytic activity that was lower than that of the commercial available catalyst.

The present work

The final goal of this thesis is enhancement of the electrochemical activity of the Pt/C catalyst prepared by the IL-sputtering method with no loss of the durability currently obtained. The simplest idea would be formation of electronic conducting paths in the IL layer between a Pt nanoparticle and a carbon support. As explained later in detail, I expected greatly use of the

protic molten salt (PMS) as a medium, on which Pt sputtering was conducted. With utilization of proton conduction of the protic molten salt, Watanabe, et al, succeeded fabrication of a fuel cell system with PMS alone as an electrolyte.[65,66] On the other hand, heat decomposition of PMS was found to result in carbonization with high yield.[67,68] Based on the functions of PMS newly focused, I started my research work aiming at improvement of the electrocatalytic performance of Pt/C prepared by the IL-sputtering method.

This thesis consists of three chapters as follows:

Chapter 1 describes preparation of the Pt/C catalysts using PMS including heating process at 1273 K with expectation of carbonization of the PMS existing between a Pt nanoparticle and a carbon supporter. The electrocatalytic activity and durability of the prepared Pt/C catalysts were compared to know effect of PMS on the Pt/C performance.

Chapter 2 describes the effect of PMS on the electrocatalytic performance of the Pt/C catalysts prepared without the heating process. Interestingly, non-heated Pt catalyst prepared using PMS showed high durability as well as remarkable mass activity. The hypothesis was proposed that this improvement behavior was ascribed to formation of the conductive polymer through electrochemical oxidation of PMS between Pt and carbon.

Chapter 3 describes verification of the hypothesis given in chapter 2. If the formation of conductive polymer by the electrochemical oxidation of PMS was a main reason why the electrocatalytic activity of the Pt/C was enhanced, addition of other monomers, oxidation of which gives a conducting polymer would work in place of the polymerizable PMS. Aniline, thiphene, and pyrrole were used for this purpose.

Chapter 1

Effect of Protic Molten Salt on Electrocatalytic Performance of the Heated Pt/C Catalyst

1-1. Introduction

Protic molten salt (PMS) and protic ionic liquid (PIL) are salts easily synthesized by the simple stoichiometric neutralization of Brønsted acid and Brønsted base, and have active proton on the cation.[65-74] They are a cost-effective option and often show desirable physicochemical properties over commonly-used ILs. It has been studied to apply PIL as a fuel cell electrolyte under non-humidifying condition,[65,66,69] and as a stabilizer for the micelle[70,71] and the protein.[72,73] As other distinctive feature, it is known that PMS and PIL comprising sulfuric acid and amine are efficiently carbonized under an Ar atmosphere (Figure 1-1).[67,68] This unique feature of PMS and PIL is focused in this study. Specifically, by heating Pt/C catalysts prepared using PMS/PIL, it is expected that the carbonization of PMS and PIL reduce the charge transfer resistance between Pt and the carbon support, improving catalytic activity (Figure 1-2). I particularly focused on diphenyl ammonium hydrogen sulfate ([DPA][HSO_4]), which shows high carbonaceous residue yield at 1273K, among the series of PMS. Because sputtering to prepare Pt nanoparticles requires liquid, Pt sputtering was performed using *N*,*N*-diethyl-*N*-methylammonium hydrogen sulfate ([DEMA][HSO_4]) which is PIL in the same

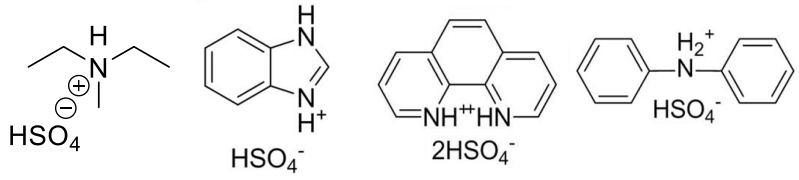

Carbonaceous residue yield at 1273K	5.4 %	16.9 %	36.5%	46.0 %

Figure 1-1. Chemical structures and carbonaceous residue yield at 1273K of several ammonium hydrogen sulfate salts.[67]

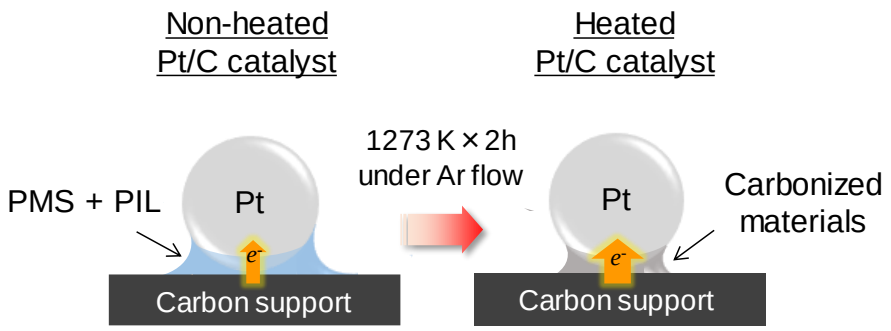

Figure 1-2. Schematic illustration of variations in the Pt nanoparticle-supported carbon electrocatalyst prepared in IL after the heating process.

series, and [DPA][HSO_4] is added to the Pt-sputtered [DEMA][HSO_4] to prepare Pt/C catalyst. In chapter 1, the elecrtocatalytic activity and durability of the Pt/C catalysts prepared using PMS and PIL including heating process at 1273 K are compared. The effect of PMS on the Pt/C electocatalytic performance is discussed to improve electrocatalytic performance of Pt/C catalyst utilizing PMS/PIL carbonization process to take advantage of unique feature of PMS/PIL.

1-2. Experimental section

1-2-1. Materials

N,*N*-diethyl-*N*-methylamine (99%), diphenylamine (98.5%) were obtained from Tokyo Chemical Industry Co., Ltd. Sulfuric acid (95%) were obtained from Wako Pure Chemicals Co., Ltd.

1-2-2. Preparation of PMS and PIL

The PMS, diphenylammonium hydrogen sulfate ([DPA][HSO_4]), and PIL, *N*,*N*-diethyl-*N*-methylammonium hydrogen sulfate ([DEMA][HSO_4]), were synthesized by simple stoichiometric neutralization reactions between amines and sulfuric acid in organic or aqueous solutions, followed by solvent removal under vacuum.[67,68]

[DPA][HSO_4]: Diphenyl amine (13.51 g, >98wt%) dissolved in 40 mL of ethanol was gradually added into a dilute sulfuric acid solution (8.24 g, 95wt% in 60 mL of ethanol) under a N_2 atmosphere in a round-bottom flask kept in an ice-water bath. The mixture was stirred for 2 h at room temperature. Finally, the solvent was removed under vacuum using a rotary evaporator at 333 K. A white powder was obtained.

[DEMA][HSO_4]: Diethyl methyl amine (9.38 g, >98 wt%) dissolved in 40 mL of ultrapure water was gradually added into a dilute sulfuric acid solution (10.37 g, 95 wt% in 60 mL of ultrapure water) under a N_2 atmosphere in a round-bottom flask kept in an ice-water bath. The mixture was stirred for 2 h at room temperature. Finally, the solvent was removed under vacuum using a rotary evaporator at 333 K. A clear, colorless liquid was obtained.

1-2-3. Preparation of the heated Pt/C catalysts

A piece of soda glass (2.5 cm × 2.5 cm) spread with [DEMA][HSO_4] (0.4 mL) was placed in a Cressington 108 Auto/SE sputter coater. A polycrystalline Pt plate target (5.7 cm diameter, 99.98%) was placed 4.5 cm above the glass plate. Sputter deposition of Pt onto [DEMA][HSO_4] was conducted with a sputter current of 40 mA in a dry Ar (99.999%) atmosphere with a pressure not exceeding 7 ± 1 Pa. The magnetron sputtering was performed in direct current (DC) mode at room temperature (298 ± 2 K) for 30 min. Carbon black (1.5 mg, Cabot, Vulcan®-XC72) was mixed and stirred with 1.2 mg of [DPA][HSO_4] in a vial containing the Pt-sputtered [DEMA][HSO_4] (0.4 mL) at 373 K for 20 min to obtain a monodispersed mixture. This mixture was agitated at 473 K for 2 h to support Pt nanoparticles on the carbon support, Vulcan®, washed with ethanol several times after the agitation process, and vacuum dried for 15 h to obtain catalyst **1**. Catalyst **2** was prepared by agitating 0.4 mL of Pt-sputtered [DEMA][HSO_4] and 1.5 mg of Vulcan® at 473 K for 2 h, and then, the mixture was washed with ultrapure water several times. A commercially available Pt-nanoparticle catalyst (TEC10V30E, Tanaka Kikinzoku Kogyo, catalyst **3**) was employed for comparison. Catalysts **4**, **5**, and **6** were

prepared by heating catalysts **1**, **2**, and **3**, respectively, at 1273 K for 2 h in a tube furnace under an Ar gas flow of 300 ml min^{-1} (Fig. 1-1). The rate of temperature increase was 10 K min^{-1}.

1-2-4. Characterization of the heated Pt/C catalysts

The morphologies of all the catalysts used in this investigation were examined using a Hitachi H-7650 transmission electron microscope (TEM), and the morphology of carbonized PMS and PIL were observed by a Hitachi S-3400N scanning electron microscope (SEM). The mean particle size of Pt was determined by measuring the size of at least 100 particles in the TEM images and calculating the average. Platinum contents in the catalysts were analyzed by a Shimadzu ICPS-7510 inductively coupled plasma atomic emission spectrometer (ICP-AES). The crystal structure of the catalysts was identified by a Rigaku Ultima IV X-ray diffractometer.

1-2-5. Electrochemical measurements

The electrocatalytic activities of catatlyst **3-5** were examined with a Hokuto Denko HZ-7000 potentiostat/galvanostat controlled with a laptop computer. The new electrocatalysts, **4** and **5** were compared with a commercially available Pt/C catalyst, **3**. The electrochemical experiments were conducted using a three-electrode cell at room temperature. A glassy carbon (GC) rotating disk electrode (surface area: 0.196 cm^2, Pine Instruments) was used as the working electrode. The GC electrode was polished to a mirror finish with a slurry of 0.06 mm alumina and then rinsed with ultrapure water and dry ethanol before use. The catalyst ink was prepared by ultrasonically dispersing 1.48 mg of the Pt catalyst in 2-propanol (1.0 mL) for 5 min. The ink (10 μL) was uniformly spread onto the GC electrode, and the solvent was slowly evaporated in air. Then, the GC disk was covered with 10 μL of a Nafion® solution (0.1 wt%) diluted with 2-propanol to fix the catalyst on the GC disk. The obtained working electrode was set in a Pine Instruments AFMSRCE electrode rotator for the measurements. Platinum mesh was used as the counter electrode, and a Ag/AgCl double-junction electrode immersed in

saturated KCl (aq) was used as the reference electrode. An aqueous solution of 0.1 M $HClO_4$ was used as the electrolyte. All potential values in this study are referenced to the reversible hydrogen electrode (RHE). Before the electrocatalytic activity measurements, the working electrode was electrochemically cleaned by 40–100 potential sweeps between 0.05 and 1.20 V (vs. RHE) at a scan rate of 50 mV s^{-1} under a N_2 atmosphere until the cyclic voltammograms were stabilize. The electrochemical surface area (ECSA) of the Pt nanoparticles was determined by the Columbic charge for hydrogen adsorption or desorption in the cyclic voltammogram under N_2 after subtracting the double-layer charge current. The ECSA value was calculated from the following equation:

$$\text{ECSA} = \frac{Q_{\text{H}} \times 10^2}{210 \times M_{\text{Pt}}} \qquad (1)$$

where Q_{H} (μC) is the amount of charge during hydrogen adsorption/desorption.[75] For comparison, the average value for the charge associated with hydrogen adsorption/desorption monolayer formation on smooth polycrystalline Pt is 210 μC cm^{-2}. M_{Pt} (μg) is the Pt mass on the GC working electrode. The durabilities of the electrocatalysts were estimated by the standard degradation test recommended by the Fuel Cell Commercialization Conference of Japan (FCCJ).[76,77] This test overloads the cathode in a proton exchange membrane fuel cell system by potential sweeps between 1.0 and 1.5 V at 500 mV s^{-1}. Carbon corrosion occurs easily under this condition, and therefore, the durability of the cathode catalyst can be electrochemically evaluated in a short time. To obtain additional insight into the deterioration behavior, the surface retention rate for the ECSA was estimated by the following equation:

Surface retention rate for the ECSA (%)

$$= \frac{\text{ECSA estimated at each cycle } (\text{m}^2\ \text{g}^{-1})}{\text{initial ECSA } (\text{m}^2\ \text{g}^{-1})} \qquad (2)$$

The oxygen reduction reaction (ORR) measurements were performed in a 0.1 M $HClO_4$

solution using the rotating disk electrode linear sweep voltammetry (RDE-LSV) in the anodic direction with a sweep rate of 10 mV s^{-1} and five different rotation speeds (200, 400, 800, 1200, and 1600 rpm) in an O_2 atmosphere. ORR at the RDE is described by the Koutecký-Levich equation as follows:

$$\frac{1}{I} = \frac{1}{I_k} + \frac{1}{B\ \omega^{1/2}} \qquad (3)$$

$$B = 0.62\ n\ F\ A\ C^*\ D^{2/3}\ v^{-1/6}\ \omega^{1/2}$$

where I is the experimentally measured current at 0.85 V, I_k is the kinetic current, ω is the electrode rotation rate, n is the electron-transfer number, F is the Faraday constant, A is the electrode surface area, C^* is the O_2 concentration in the electrolyte, D is the diffusion coefficient of O_2 in the electrolyte, and v is the viscosity of the electrolyte. I_k was estimated from the intercept in the Koutecký-Levich plot (I^{-1} vs. $\omega^{-1/2}$). For each catalyst, the kinetic current was normalized to the Pt loading to obtain mass activities. The catalytic activity retention rate for the mass activity was obtained by an equation similar to equation (2):

Catalytic activity retention rate for mass activity (%)

$$= \frac{\text{mass activity estimated after 15,000 cycles (A g}^{-1})}{\text{initial mass activity (A g}^{-1})} \qquad (4)$$

1-3. Results and discussion

1-3-1. Characterization of the heated Pt/C catalysts

Photographs and SEM images of the [DPA][HSO_4] PMS/[DEMA][HSO_4] PIL mixture and neat [DEMA][HSO_4] PIL carbonized at 1273 K are in Figure 1-3. For the PMS/PIL mixture, a self-standing carbon foam is obtained, and the carbonaceous residue yield was ca. 42.2 wt%.

In the case of the [DEMA][HSO_4], only small amount of agglomerated small particles remains (carbonaceous residue yield: ca. 6.9 wt%). The carbonaceous residue yields are close to those reported by Watanabe et al.[67,68] These results suggest that structure and thickness of the carbon layer depend on the PMS and PIL species. In order to confirm the carbonization reaction on the Pt nanoparticle-supported carbon electrocatalysts prepared using the [DPA][HSO_4] PMS/[DEMA][HSO_4] PIL mixture, catalyst **1**, or the [DEMA][HSO_4] PIL, catalyst **2**, the catalysts before and after the carbonization process were compared by means of TEM. As a reference, a commercially available electrocatalyst, **3**, was also employed. Catalysts **4**, **5**, and **6** were prepared by heat treatment of catalysts **1**, **2**, and **3**, respectively, at 1273 K for 2 h. Figure1-4 shows TEM images of catalysts **1**−**6**. After the heat treatment, the mean particle size of the Pt nanoparticles supported on the carbon black clearly increases (Table 1-1), but a homogeneous dispersion of the nanoparticles is maintained. The mean particle sizes for **4** and

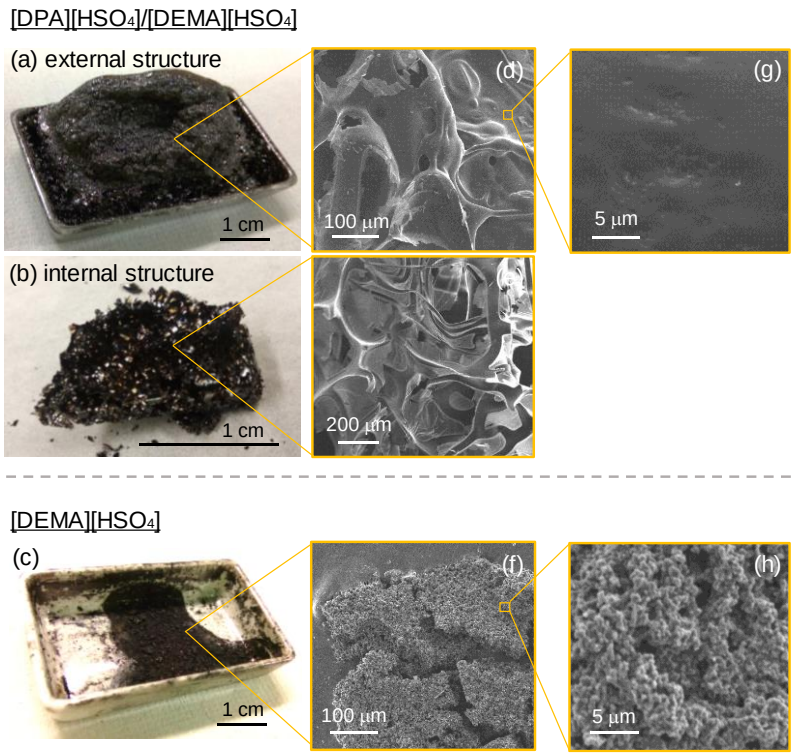

Figure 1-3. (a−c) Photographs and (d−h) SEM images of the carbonized PMS/PIL mixture and neat PIL. (a, d, g) external and (b, e) internal structures of the carbonized [DPA][HSO_4] PMS/[DEMA][HSO_4] PIL mixture (mixing weight ratio = 2 : 1), and (c, f, h) external structure of the carbonized neat [DEMA][HSO_4] PIL.

5 were 6.1 and 6.3 nm, respectively. As for **6**, the size is larger than these two catalysts (10.3 nm), although their original sizes, ca. 2.5~2.8 nm, are quite similar. The moderate Pt nanoparticle aggregation observed on the **4** and **5** may be due to the thin IL layer on the catalysts. Indeed, high magnification TEM images of **1** and **2** show that a number of Pt nanoparticles are covered with the IL layer (Figure 1-4a,b (inset)). After the carbonization process, the

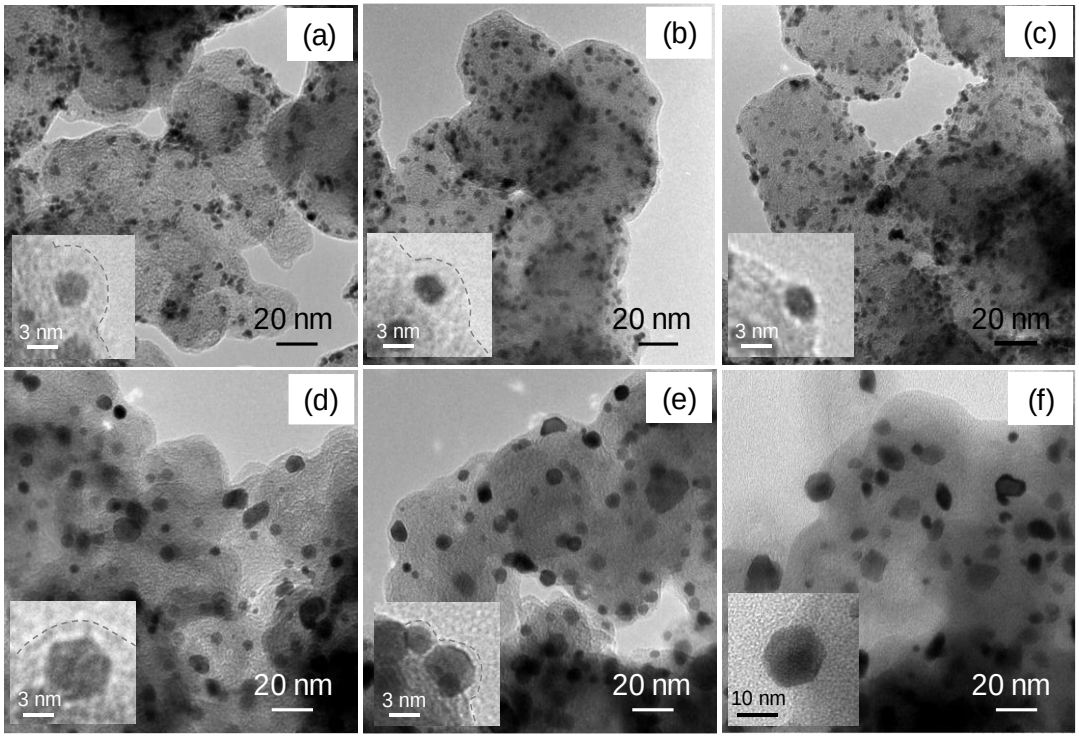

Figure 1-4. TEM images of the Pt nanoparticle-supported carbon electrocatalysts. Electrocatalysts are (a) **1**, (b) **2**, (c) **3**, (d) **4**, (e) **5**, and (f) **6**. (Insets) High-magnification TEM images of **1**−**6**.

Table 1-1. Mean particle size and loading amount of Pt of the Pt/C catalysts.

Entry	Mean particle size (nm)	Loading amount of Pt (wt%)
1[a]	2.9 ± 0.5	23.0
2[b]	2.6± 0.5	23.8
3[c]	2.6 ± 0.8	26.2
4[d]	6.1 ± 4.4	29.1
5[e]	6.3 ± 5.1	25.9

[a]**1** was prepared using [DPA][HSO_4] and [DEMA][HSO_4]. [b]**2** was prepared using [DEMA][HSO_4]. [c]TEC10V30E. [d]**4** was prepared by heating **1** at 1273 K. [e]Catalyst **5** was prepared by heating **2** at 1273 K.

nanoparticles were encapsulated by the carbonized PMS and PIL (Figure 1-4d,e), it is expected that the carbonized material structure depending on PMS and PIL species as shown in Figure 1-3 covers the surface of Pt nanoparticles in Pt/C catalyst as shown in Figure1-5. This process yields both spherical and polyhedral shaped Pt nanoparticles. Similar morphology change was recognized, when commercially-available catalyst **3** was heated under the same condition (Figur 1-4c,f). It means that the PMS and PIL are not involved in the morphology change. As depicted in Figure 1-6, the XRD patterns indicate smaller half-value widths for the Pt metal on the **4**–**6** than original catalysts **1**–**3,** since the Pt crystallite size increased *via* the heat treatment at 1273 K. On the other hand, no diffraction pattern derived from graphitic structure is observed in ones for the catalysts **4** and **5**, suggesting that carbon materials in the catalysts have amorphous structure.[67]

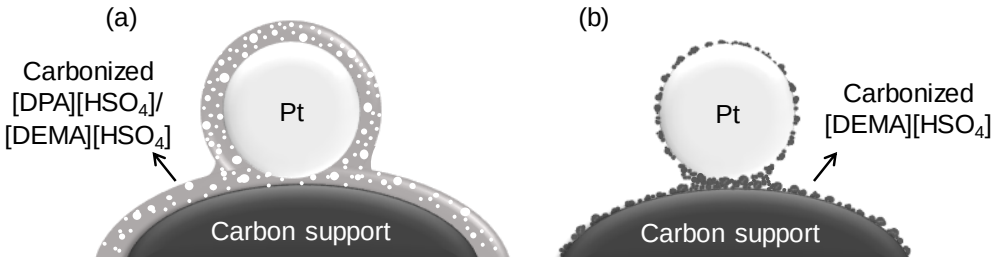

Figure 1-5. Schematic illustration of variations in the heated Pt nanoparticle-supported carbon electrocatalyst prepared using (a) [DPA][HSO_4]/[DEMA][HSO_4] and (b) [DEMA][HSO_4] after the heating process.

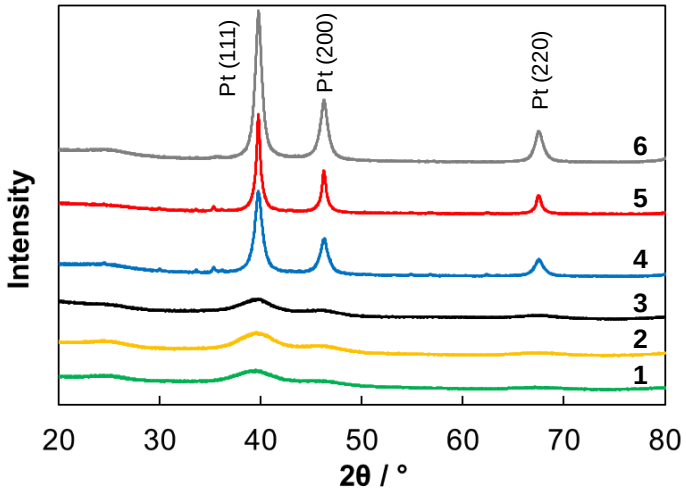

Figure 1-6. XRD patterns of the Pt-nanoparticle-supported carbon electrocatalysts.

1-3-2. Electrocatalytic performance and durability of the heated Pt/C catalysts

Figure 1-7 indicates the cyclic voltammograms recorded at the electrodes with the electrocatalysts **3**–**5**, in a N_2-saturated 0.1 M $HClO_4$ aqueous solution before and after the durability test. All the voltammograms show commonly observed electrochemical behaviors. That is, the redox waves for hydrogen adsorption/desorption and platinum oxidation/reduction appear at the potential ranges of ca. 0.10−0.35 V and ca. 0.80−1.20 V, respectively.[15-27] A pair of peaks observed at ca. 0.60 V are attributed to the redox reaction of quinone and hydroquinone moieties on the carbon materials.[78] However, at the electrodes with **4** and **5**, the current densities for hydrogen adsorption/desorption at ca. 0.10−0.35 V are smaller than commercially available catalyst **3** due to the larger Pt nanoparticles. ECSAs of three catalysts were estimated from the hydrogen desorption peak observed in the voltammograms (see details

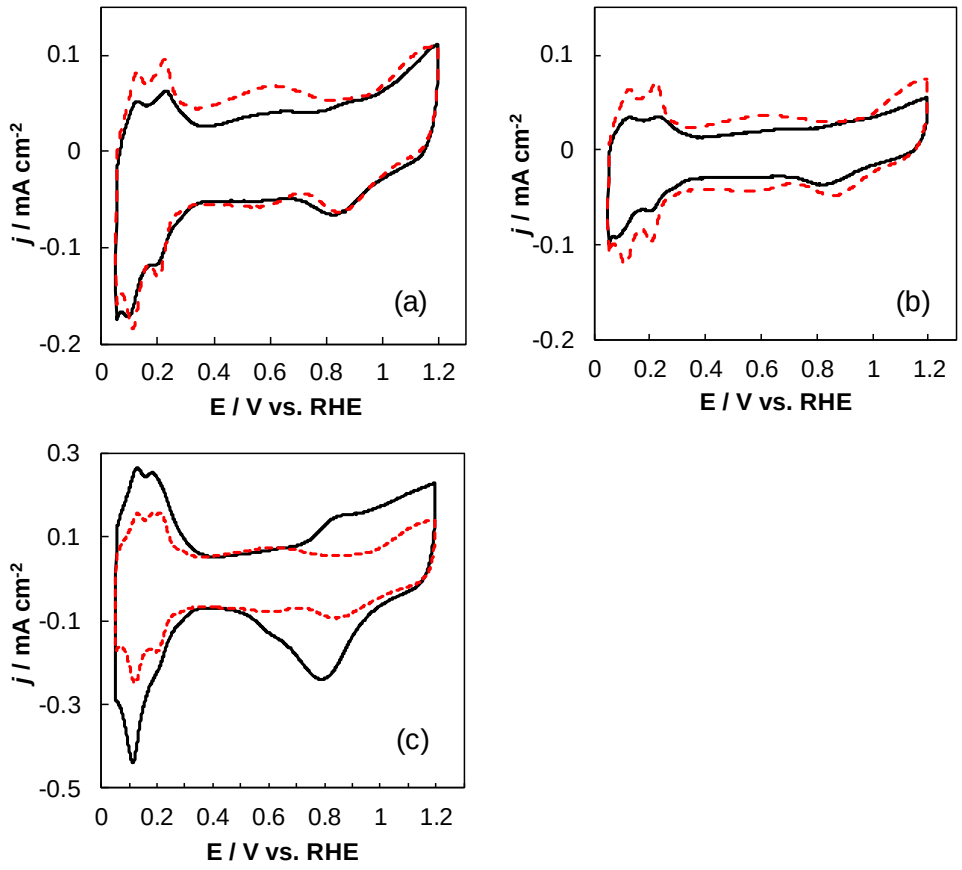

Figure 1-7. Cyclic voltammograms recorded in a N_2-saturated 0.1 M $HClO_4$ aqueous solution (—) before and (- - -) after the potential cycling tests. Sweep rate is 10 mV s^{-1}. Electrocatalysts are (a) **4**, (b) **5**, and (c) **3**.

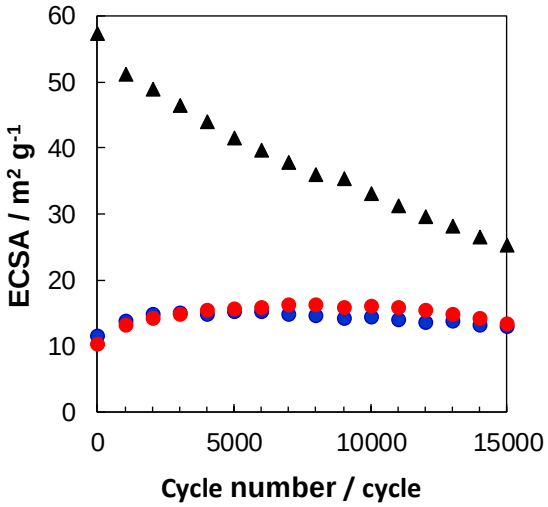

Figure 1-8. Variation in the ECSA as a function of cycle number. Electrocatalysts are (▲) **3**, (●) **4**, and (●) **5**.

in the Experimental section), ECSAs before and after durability test and surface retention rates for ECSA are summarized in Table 1-2. Figure 1-8 plots ECSAs for **3**–**5** as functions of the cycle number. As expected from the voltammograms in Figure 1-7, the initial ECSAs for **4** and **5** are very low, 11.4 and 10.3 m^2 g^{-1}, respectively (Table 1-2), but, during the durability test, their ECSAs are stable without significant change. The encapsulation of Pt nanoparticles by the carbonized PMS/PIL would relate to the high stability. These two catalysts exhibited exceptionally high surface retention rates of 112.2 and 129.0 %, respectively. Considering that the redox waves associated with the quinone-like structure, which come from carbon corrosion, become clearer after the durability test compared to other three catalysts, probably the carbon corrosion of the carbonized PMS/PIL layer on the Pt nanoparticles during the cycle test made it possible to expose Pt surface to the aqueous solution directly and resulted in the increase in electrochemically active area.

The ORR performance of **3**–**5** was examined by the RDE-LSV in an O_2-sataurated 0.1 M $HClO_4$ before and after the cycle test (Figure 1-9). Their mass activities and specific activities were calculated from the current density at 0.85 V and Pt loading. These data are summarized in Figure 1-10a and Table 1-2. The low initial ECSAs for **4** and **5** relate to insufficient initial mass activities. Surprisingly the mass activity for **4** improves after the 15,000-cycle test. It

should be attributable to the increase in O_2 diffusion routes derived from the aforementioned carbon corrosion of the carbonized PMS/PIL during the durability test. The mass activitiy retention rate for **4** is much higher (245.9% at 15,000 cycle) than the other catalysts, and the mass activity remains virtually unchanged up to 45,000 cycles. Sufficient encapsulation of Pt nanoparticles by the carbonized [DPA][HSO_4]/[DEMA][HSO_4] plays a role in unexpected result. However, the mass activity of **5** functionalized by the carbonization process similar to **4** slightly decreases after the cycle test, because, as described above, the insufficient carbon layer originating from [DEMA][HSO_4] PIL is formed on the Pt nanoparticles. From the data given in Table 1-2, specific activity was also estimated (Figure 1-10b). The initial specific activity for **4** is comparable to commercially available catalyst **3**. After the cycle test over more than

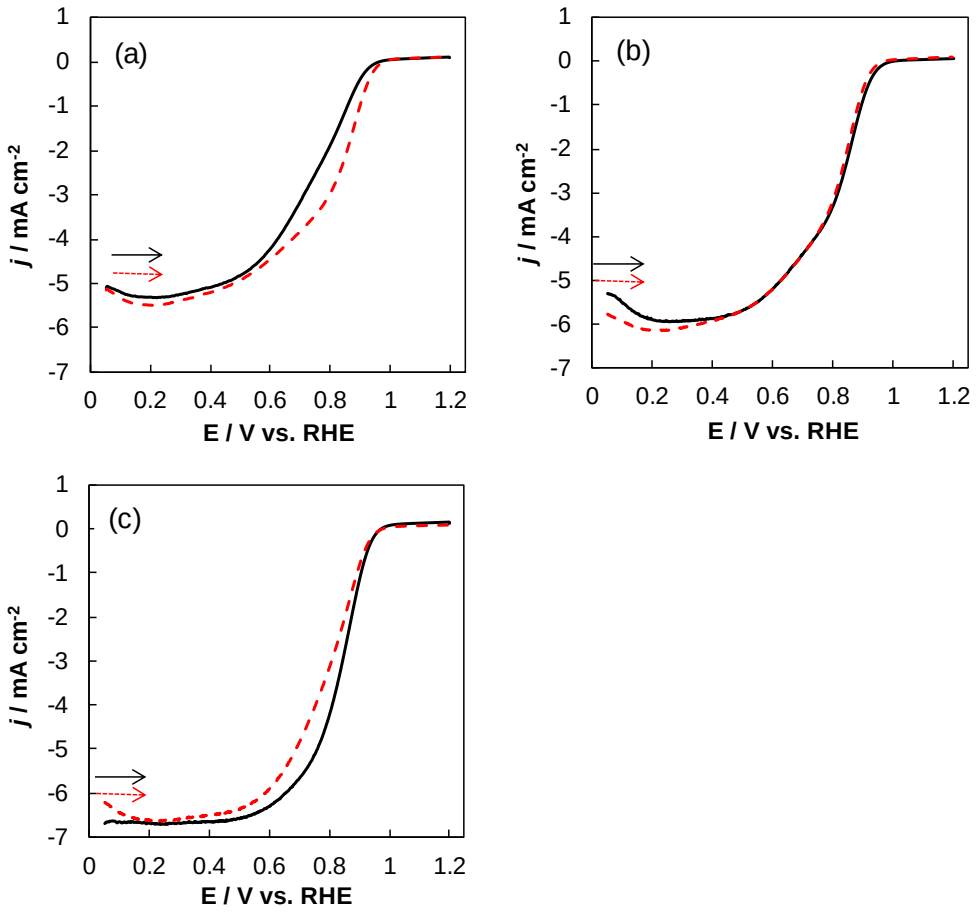

Figure 1-9. Hydrodynamic voltammograms recorded at RDEs with different electrocatalysts (—) before and (- - -) after the durability test in an O_2-saturated 0.1 M $HClO_4$ at 1,600 rpm. The scan rate is 10 mV s^{-1}. Electrocatalysts are (a) **4**, (b) **5**, (c) **3**.

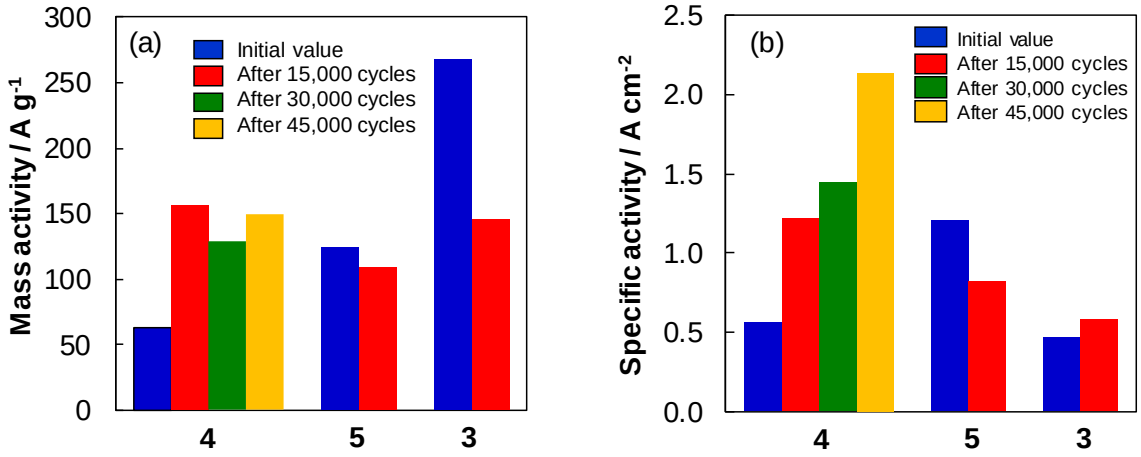

Figure 1-10. Comparison of (a) the mass activities and (b) the specific activities recorded at **3**–**5** before and after the potential cycling tests.

15,000 cycle, **4** exhibits the highest value among the **3**−**5**, and the specific activity for **4** finally reaches 2.1 mA cm^{-2} after 45,000 cycles. These results, reveal that the carbonized layer formed by the [DPA][HSO_4]/[DEMA][HSO_4] mixture greatly enhances both catalytic durability and specific activity.

Table 1-2. Summary of the Pt nanoparticle-supported carbon electrocatalysts discussed on catalytic activity in this chapter.

Entry	PMS/PIL species	ECSA			Mass activity			Specific activity	
		Initial ($m^2\ g^{-1}$)	After 15,000 cycle ($m^2\ g^{-1}$)	Surface retention rate (%)	Initial ($A\ g^{-1}$)	After 15,000 cycle ($A\ g^{-1}$)	Catalytic activity retention rate (%)	Initial ($mA\ cm^{-2}$)	After 15,000 cycle ($mA\ cm^{-2}$)
4[a]	[DPA][HSO_4]/ [DEMA][HSO_4]	11.4	12.8	112.2	63.5	156.1	245.9	0.56	1.22
5[b]	[DEMA][HSO_4]	10.3	13.3	129.0	124.2	109.3	88.0	1.20	0.82
3[c]	-	57.8	27.2	47.1	264.4	144.6	54.7	0.46	0.53

[a]**4** was prepared by heating **1** at 1273 K. [b]**5** was prepared by heating **2** at 1273 K. [c]**3** TEC10V30E.

1-4. Conclusions

The carbonization of the [DPA][HSO_4] PMS/[DEMA][HSO_4] PIL mixture on the ORR electrocatalysts prepared using the Pt nanoparticle-monodispersed IL enables a high specific activity up to 2.1 mA cm^{-2} after the 45,000 cycle test because of the improvement of the charge transfer ability between Pt nanoparticles and carbon support by the formation of a fine carbonized PMS/PIL layer. Sufficient encapsulation of Pt nanoparticles on the carbon support is necessary to realize electrocatalysts with a long-term stability. But moderate carbon corrosion of the carbonized PMS/PIL layer on the Pt nanoparticles is effective for O_2 diffusion routes, i.e., for obtaining a better catalytic property. The findings reported in this chapter offer helpful suggestions to functionalize the IL-based electrocatalysts for ORR.

Chapter 2

Effect of Protic Molten Salt on Electrocatalytic Performance of the Non-heated Pt/C Catalyst

2-1. Introduction

In order to reduce Pt cost which is one of the biggest issue of ORR catalyst, numerous efforts to reduce Pt usage and to improve catalytic activity have been conducted by various approaches,[79-90] e.g., alloying Pt nanoparticle with transition metals,[79-83] crystallographic control of Pt nanoparticles,[84-87] utilization of ionic liquids (ILs) with high oxygen solubility,[88] and Pt surface modification by specific amine capping.[89,90]

The Pt/C catalyst described in chapter 1 was heated to carbonize PMS/PIL in Pt/C catalyst. The heating of Pt/C with PMS catalyst drastically improves the specific activity, however on the other hand leaves a problem of enlarging Pt and consequently reducing the mass activity. In order to improve of mass activity for the heated Pt/C catalyst, it is necessary to suppress the aggregation of the Pt nanoparticles. As one way to solve that, the catalytic performance of the non-heated Pt/C catalyst prepared by adding [DPA][HSO_4] to Pt-sputtered [DEMA][HSO_4], catalyst **1**, was examined. Interestingly it was found that **1** showed remarkable higher mass activity than the heated one and commercially available Pt-nanoparticle catalyst. Therefore, based on this result, the effect of PMS, [DPA][HSO_4], on the electrocatalytic performance for the non-heated Pt/C catalyst was investigated and the hypothesis to improve electrocatalytic performance of non-heated Pt/C catalyst by PMS was proposed to disclose novel approach for the enhancement of catalytic activity.

2-2. Experimental section

2-2-1. Preparation of the non-heated Pt/C catalysts

The non-heated Pt/C catalyst, catalyst **1** prepared using [DPA][HSO_4] and [DEMA][HSO_4], [DPA][HSO_4] free catalyst **2** shown in chapter 1 were prepared without heating process. Similarly, the Pt/C catalyst with commonly used IL, trimethylpropylammonium bis(trifluoromethanesulfonyl)amide ([$N_{1,1,1,3}$][Tf_2N]), was also prepared. [$N_{1,1,1,3}$][Tf_2N] were purchased from Kanto Chemical Co., Inc. and was purified before use with a method previously described in the literature.[91] Catalyst **7** was prepared by agitating 0.4 mL of Pt-sputtered [$N_{1,1,1,3}$][Tf_2N] and Vulcan® at 573 K for 2 h to support Pt nanoparticles on the carbon support, followed by washing with acetonitrile several times. Catalyst **8** was prepared by mixing 2.0 mg of TEC10V30E (Catalyst **3**), 0.1 g of [DEMA][HSO_4], and 0.3 g of [DPA][HSO_4] at 473 K for 2 h and then rinsing with ethanol several times. In this chapter, catalyst **1** and **2** were compared with a catalyst prepared with [$N_{1,1,1,3}$][Tf_2N], **7**, which was reported in previous reserch,[59] as well as the commercially available catalyst TEC10V30E, **3**. Additionally, TEC10V30E heat-treated with a mixture of [DPA][HSO_4] and [DEMA][HSO_4], **8**, was also examined.

2-2-2. Characterization and electrochemical measurements

Characterization and electrochemical measurement of the non-heated Pt/C catalyst were carried out in the same method as in chapter 1.

2-3. Results and discussion

2-3-1. Characterization of the non-heated Pt/C catalysts

Figure 2-1 shows the TEM images and size distributions of the non-heated Pt/C catalysts **1**, **2**, **3** and **7** used in this chapter. The size distributions of the nanoparticles were determined by measuring size of individual particles in the TEM images. For **1** and **2**, the Pt nanoparticles

were homogeneously dispersed on the surfaces of carbon black, Vulcan®, displaying a mean particle size of ca. 2.5-3.0 nm with the narrow size distribution, which were slightly smaller than that of **7** (3.6 nm) and equivalent to that of **3** (2.6 nm). The Pt loading amount on catalysts **1**, **2** and **7** was ca. 23~24%, which was lower than that for **3** (ca. 26%). These data are summarized in Table 2 along with electrocatalytic properties that will be described later.

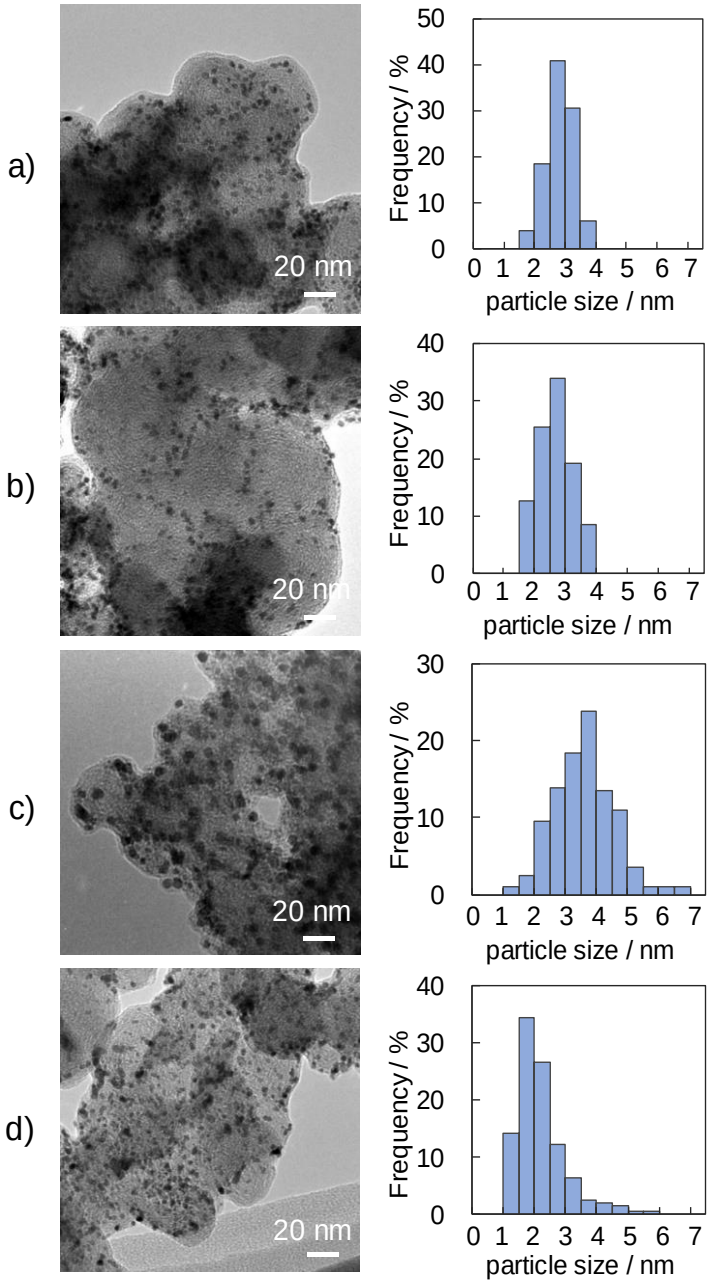

Figure 2-1. TEM images of the non-heated Pt nanoparticle-supported carbon electro catalysts used in this chapter and their size distribution data: a) **1**, b), **2**, c) **7**, and d) **3**.

Table 2. Summary of the non-heated Pt nanoparticle-supported carbon electrocatalysts used in this chapter.

Entry	Used salt and IL species	Mean particle size (nm)	Pt loading amount (wt%)	ECSA				Mass activity			$\Delta E_{1/2}$ [a] (mV)
				Initial ($m^2 g^{-1}$)	Maximum ($m^2 g^{-1}$)	After 15,000 cycles ($m^2 g^{-1}$)	Surface retention rate (%)	Initial (A g^{-1})	After 15,000 cycles (A g^{-1})	Catalytic activity retention rate (%)	
1	[DPA][HSO_4] + [DEMA][HSO_4]	2.9 ± 0.5[b]	23.0	42.1	51.1	43.6	103.5	436.1	498.1	114.2	- 6
2	[DEMA][HSO_4]	2.6 ± 0.5[b]	23.8	44.6	51.1	36.0	80.7	255.2	224.5	88.0	8
7	[$N_{1,1,1,3}$][Tf_2N]	3.6 ± 1.0[b]	23.2	45.8	49.3	36.6	79.9	165.2	134.9	81.6	1
3[c]	-	2.6 ± 0.8[b]	26.2	51.3	51.3	15.5	30.2	273.7	173.6	63.4	41
8	[DPA][HSO_4] + [DEMA][HSO_4] with **3**	2.8 ± 1.0[b]	22.1	38.4	38.4	18.3	47.7	258.2	157.3	60.9	58

[a] $\Delta E_{1/2}$ shows the difference in the half-wave potential before and after the potential cycling test estimated from Figure 2-5. [b] The values in parentheses show the standard deviation. [c] **3** TEC10V30E.

2-3-2. Electrocatalytic performance and durability of the non-heated Pt/C catalyst

Figure 2-2 shows the cyclic voltammograms recorded at electrocatalysts **1**, **2**, **3** and **7** in a N_2-saturated 0.1 M $HClO_4$ aqueous solution before and after a potential cycling test (15,000 cycles) that simulates actual fuel cell operation. For all the catalysts, the redox waves for hydrogen adsorption/desorption and platinum oxidation/reduction appeared at the potential ranges of 0.10 ~ 0.35 V and 0.80 ~ 1.20 V, respectively. A pair of ill-defined peaks appeared at approximately 0.60 V due to the redox reaction of the quinone and hydroquinone moieties on the carbon support.[78] Furthermore, the Pt-oxide reduction peak potentials positively shifted

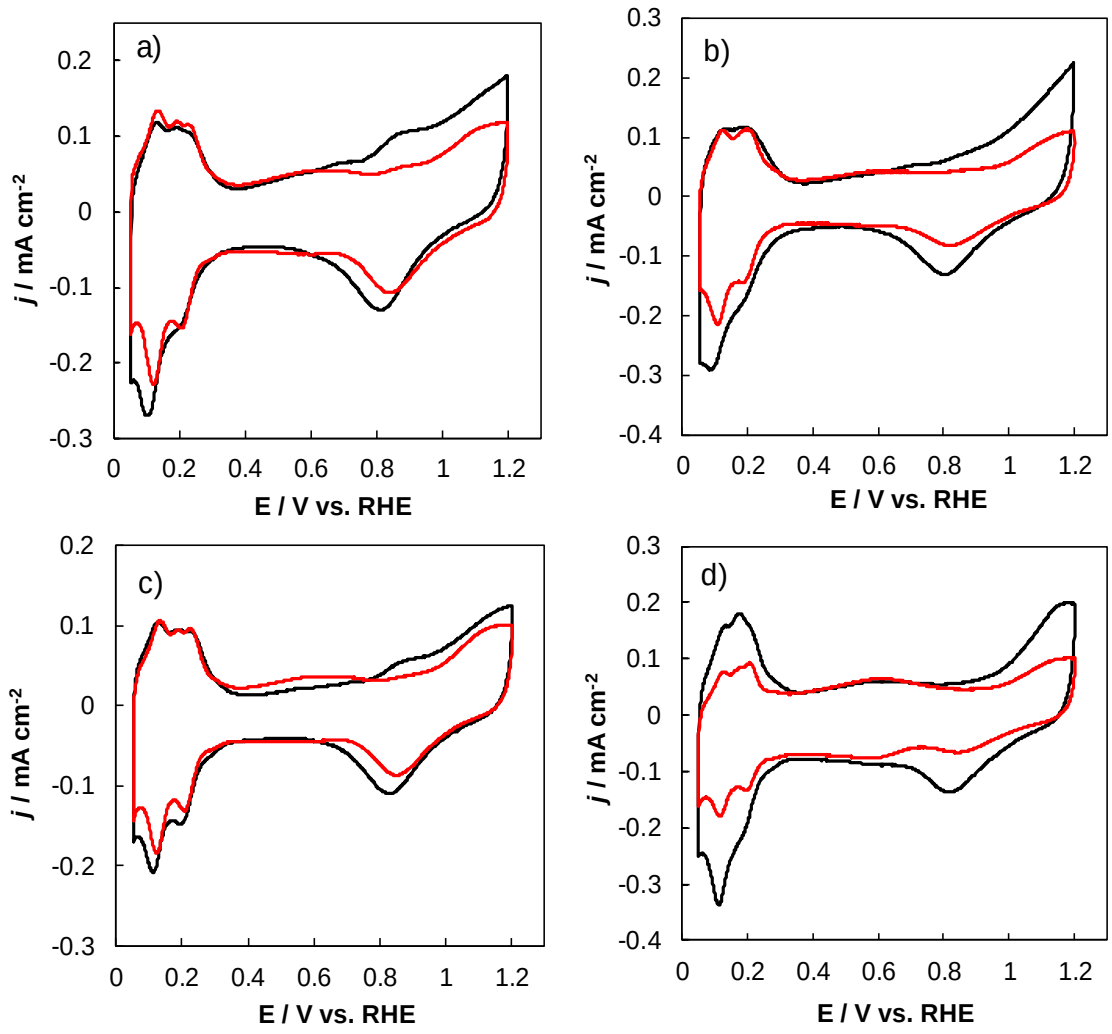

Figure 2-2. Cyclic voltammograms recorded at a) **1**, b) **2**, c) **7**, and d) **3** in a N_2-saturated 0.1 M $HClO_4$ aqueous solution before (——) and after (- - -) the durability tests.

after the cycling tests. This positive shift of the reduction peak is due to the weaker adsorption strength of the oxygen-containing chemical species on the metal surface, which is caused by an increased Pt particle size,[92] i.e., related to the binding strength of oxygen on the metal surface. ECSAs of all the catalysts were estimated from the hydrogen desorption peak observed in the voltammograms. The obtained values are given in Table 2. Compared to the commercially available catalyst **3**, the other three catalysts prepared with ILs showed smaller initial ECSAs (Table 2) due to residual IL on the Pt nanoparticles meagerly preventing the adsorption of H atoms.[93,94]

Changes in the ECSA during potential cycling tests have provided important insights into the durabilities of catalysts. Figure 2-3 shows the ECSA and the surface retention rate for the ECSA as a function of cycle number. While **3** had the highest initial ECSA of 51.3 m^2 g^{-1}, this value decreased rapidly to 15.5 m^2 g^{-1} after 15,000 cycles (retention rate: 30.2%). In contrast, for catalysts **1**, **2** and **7** prepared using ILs, their ESCAs increased during the initial several thousand cycles and gradually decreased after reaching maximum values. The anomalous increase in the ECSA is caused by the desorption of residual IL on the Pt nanoparticles during the potential cycling test.[59] Catalysts **1**, **2** and **7** maintained much higher surface retention rates

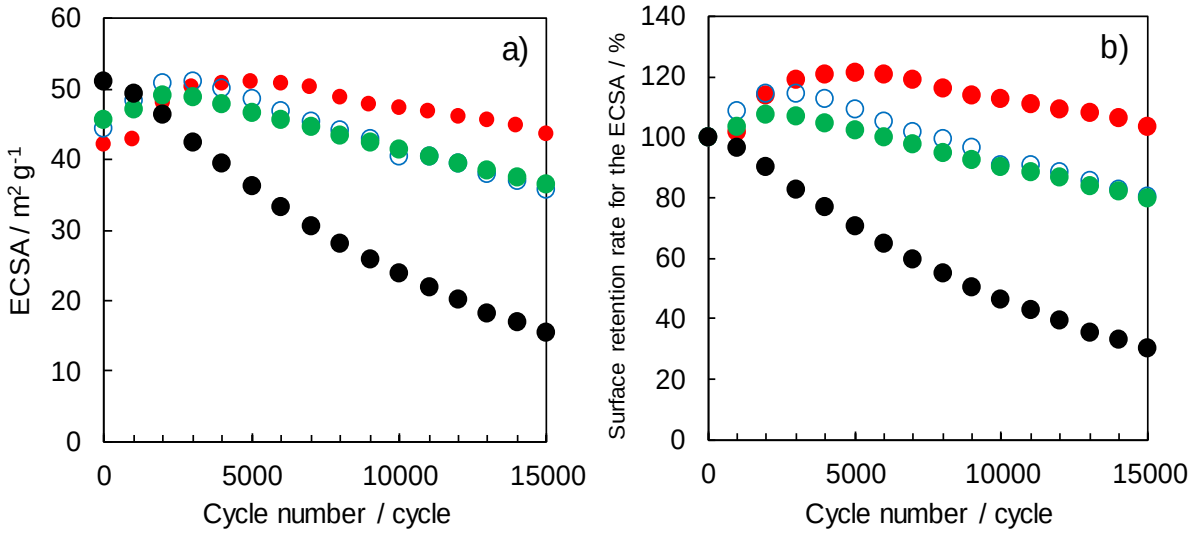

Figure 2-3. Variation in the a) ECSA and b) surface retention rate for the ECSA estimated from Figure 2-3a as a function of cycle number: ●) **1**, ○) **2**, ■) **7**, and ▲) **3**.

(approximately 80 to 104%) even after 15,000 cycles, and it is interesting that the ECSA for the catalyst **1** after the cycling test became a larger value compared to the initial one. Carbon corrosion typically proceeds during the potential cycling test *via* the oxidation of functional groups on the carbon support to CO_2 and CO.[6-13] Recently, it was reported that a thin IL layer, which exists between the Pt nanoparticles and the carbon support, prevents this corrosion.[59] The high durabilities of **2** and **7** are explained by the same phenomenon. For the higher surface retention rate of the catalyst **1**, it is considered that not only the IL layer effect but also the addition of [DPA][HSO_4] as discussed later promote the suppression of carbon-support corrosion and the agglomeration of Pt nanoparticles. TEM observations of the electrocatalysts after the potential cycling tests were conducted to visually understand the deterioration (Figure 2-4). Some degree of aggregation of the Pt nanoparticles after the cycling test was recognized in each case. However, for the three catalysts prepared using ILs, many Pt nanoparticles remained on the carbon support. In contrast, the number of Pt nanoparticles on **3** clearly

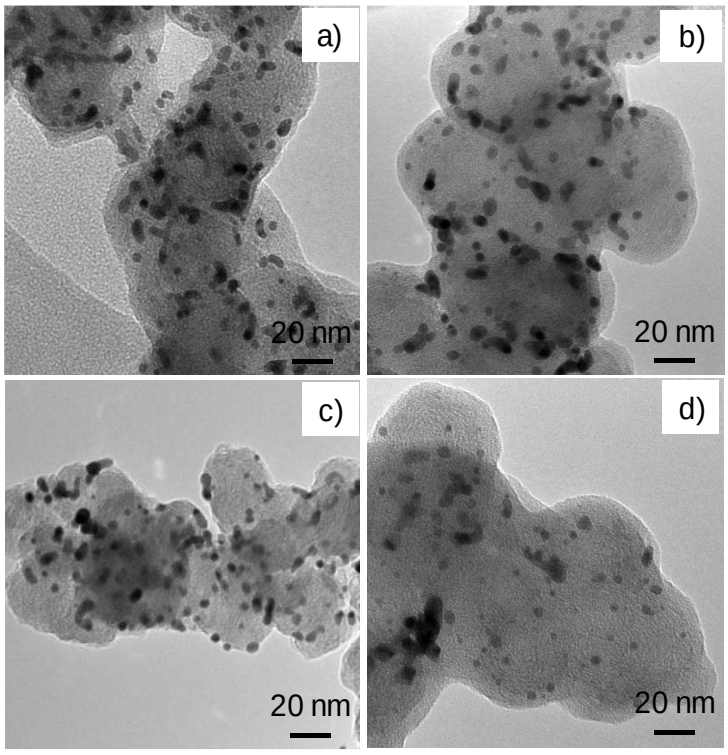

Figure 2-4. TEM images of the Pt-nanoparticle-supported carbon electrocatalysts after the durability tests (15,000 cycles): a) **1**, b) **2**, c) **7**, and d) **3**.

decreased due to nanoparticle detachment caused by deterioration of the carbon support.[6-13] These results are consistent with the retention rate trends of the ECSA.

The electrocatalytic mass activity is an essential measure for evaluating ORR electrocatalysts. The ORR performances of specimens **1**, **2**, **3** and **7** were examined by the RDE-LSV (Figure 2-5), and their mass activities at 0.85 V were calculated. Surprisingly, **1** showed a very high initial mass activity exceeding that of the commercially available catalyst **3**. In comparison with **2**, [DPA][HSO_4] enhanced the mass activity of **1**. Even the initial mass activity of **2** without the [DPA][HSO_4] was nearly 1.5 times higher than that of **7** obtained from the common [$N_{1,1,1,3}$][Tf_2N] IL. The difference in the mass activity was not due to the ECSA, as the ECSAs of **2** and **7** are roughly equivalent but was attributed to the higher affinity between

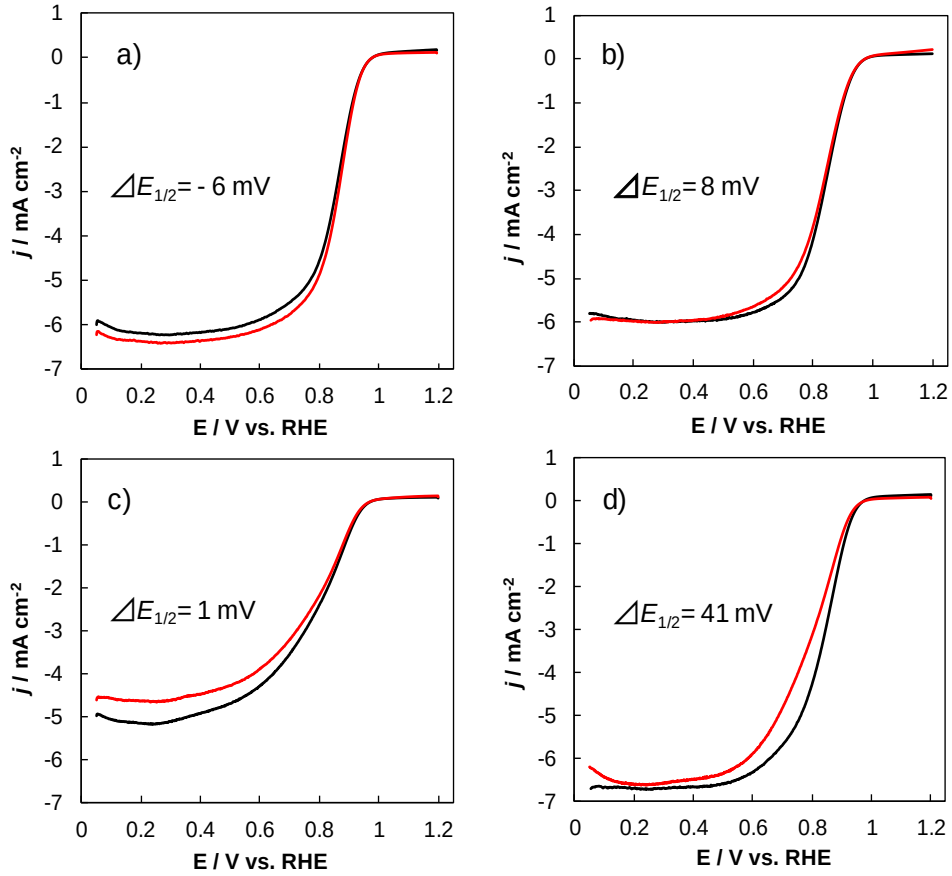

Figure 2-5. Hydrodynamic voltammograms recorded at RDEs with electrocatalysts before (—) and after (- - -) the durability test in an O_2-saturated 0.1 M $HClO_4$ at 1,600 rpm. The scan rate was 10 mV s^{-1}. Electrocatalysts are a) **1**, b) **2**, c) **7**, and d) **3.** The $\Delta E_{1/2}$ value shows the change in the half-wave potential before and after the potential cycling test.

the hydrophilic IL, [DEMA][HSO_4], and the carbon materials (carbon support or glassy carbon electrode). Notably, the mass activity of **1** increased after 15,000 cycles, whereas those of the other three catalysts decreased (Figure 2-6). The catalytic activity retention rates on the mass activity for **1**, **2**, **7**, and **3** were 114.2%, 88.0%, 85.5%, and 63.4%, respectively (Table 2). The apparent deterioration of **3** was recognized, and for **2** and **7**, a moderate deterioration rate was observed, as reported in previous paper of the group which the author belongs.[59] The differences in the half-wave potential ($\Delta E_{1/2}$) estimated from the RDE-LSVs are displayed in Figure 2-5. Only **1** showed a positive shift of the half-wave potential after the cycling test, whereas the other three catalysts showed negative shifts. This positive shift indicates that an unexpected reaction occurred on **1** during the cycling test and enhanced the catalytic properties. The origin for this enhancement must be [DPA][HSO_4], as **2** prepared using [DEMA][HSO_4], which was the same IL used for **1**, but without [DPA][HSO_4], did not show such enhancement. One plausible explanation for this behavior is the formation of a conductive polymer, poly(diphenylamine), during the electrochemical cleaning process conducted prior to the voltammetric measurements and the potential cycling tests. In fact, poly(diphenylamine) (conductivity: $1.5 \times 10^{-2} \sim 5 \times 10^{-1}$ Ω^{-1} cm^{-1}) can be produced by an electrochemical

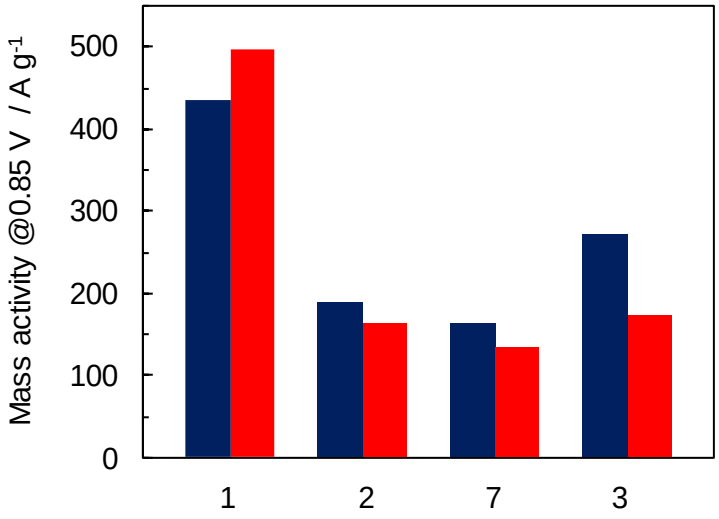

Figure 2-6. Comparison of mass activities recorded at **1**, **2**, **3**, **7** before (blue) and after (red) the potential cycling tests (15,000 cycles).

polymerization reaction in an acidic aqueous solution with diphenylamine.[95-100] This reaction can also occur for [DPA][HSO_4] in the mixture layer existing between the Pt nanoparticles and the carbon support, as the electrochemical oxidation of $[DPA]^+$ was conducted in a 0.1 M $HClO_4$ aqueous solution, which meets the polymerization conditions for diphenylamine. This plausible polymerization process is summarized in Figure 2-7 and schematically illustrated in Figure 2-8. The conductive poly(diphenylamine) formed reduces the charge-transfer resistance between the Pt nanoparticles and the carbon support, greatly improving the mass activity and durability of **1** after the potential cycling test. Besides, it is linked to the superior ECSA retention rate, too. Interestingly, even when **3** was covered with the [DPA][HSO_4] and [DEMA][HSO_4] mixture, i.e., catalyst **8**, the catalytic properties remained similar to **3** (Table 2), suggesting that the PMS and PIL mixture had to exist between the Pt nanoparticles and the carbon support for enhanced activity.

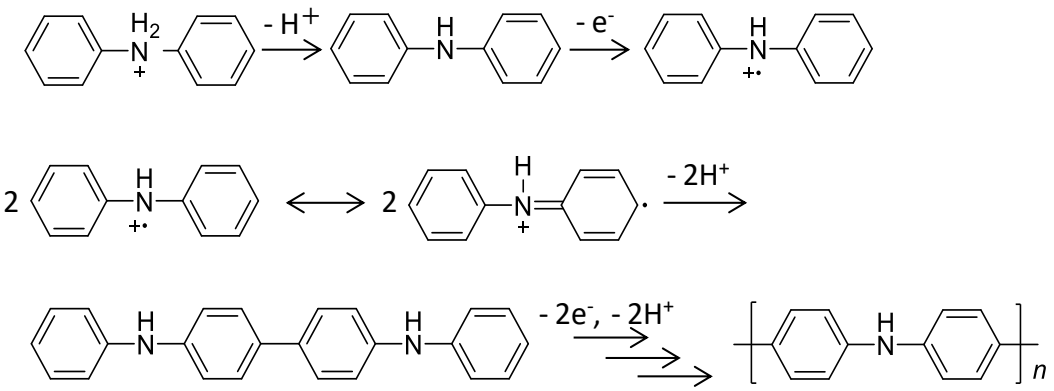

Figure 2-7. Plausible electrochemical polymerization process of [DPA][HSO_4].

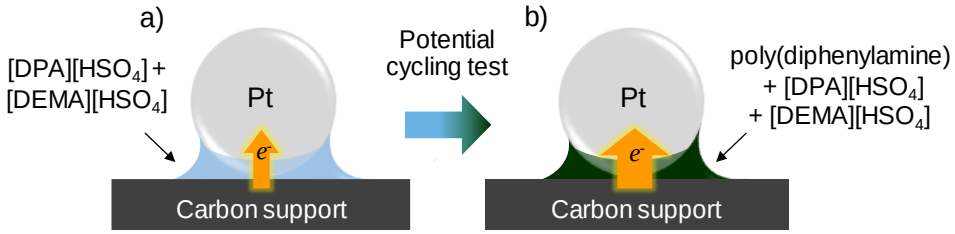

Figure 2-8. Schematic illustration of the change in Pt nanoparticle-supported carbon electrocatalyst **1** prepared in this study a) before and b) after the potential cycling test.

2-4. Conclusions

In conclusion, highly functional Pt-nanoparticle-supported carbon electrocatalysts using PMS and PIL were successfully fabricated. The resulting electrocatalyst prepared from a mixture of [DPA][HSO_4] and [DEMA][HSO_4] showed very high durability and remarkable mass activity. The catalytic properties largely surpassed those of a commercially available catalyst and previously synthesized catalysts produced using ILs in the group which the author belongs. $[DPA]^+$ provides further functionality to the electrocatalyst but required to be positioned between the Pt nanoparticles and the carbon support. The approach reported in this chapter will be a useful technique and provide valuable insight for improving future ORR electrocatalysts.

Chapter 3

The Mechanism for Improvement of Electrocatalytic Performance using Protic Molten Salt

3-1. Introduction

As discribed in chapter 2, the Pt/C catalyst prepared using a polymerizable PMS, [DPA][HSO_4], showed anomalously high catalytic behavior that gradually appeared during the potential cycling test, leading to propose hypothesis that this unexpected result was possibly ascribed to the formation of a conductive polymer, poly(diphenylamine), by the electropolymerization of [DPA][HSO_4] in an IL layer between the Pt nanoparticles and the carbon support. As electropolymerized conductive polymers,[101-103] polyaniline,[104-106] polypyrrole,[107-109] and polythiophene [110-112] are well known besides polydiphenylamine. It is, therefore, expected that the electrocatalytic performance is enhanced by formation of these conductive polymers in Pt/C catalyst. The validation of the above hypothesis of improvement of electrocatalytic performance by PMS was tested to establish a fabrication process for the long-life Pt/C catalyst with a favorable catalytic activity. For this purpose, the change of [DPA][HSO_4] by potential cycling and the effect of several electropolymerizable additives to form polyaniline, polythiophene, and polypyrrole on the electrocatalytic performance of Pt/C catalyst were investigated.

3-2. Experimental section

3-2-1. Materials

3-methylthiophene (98%, 3MT) were obtained from Tokyo Chemical Industry Co., Ltd. 3,4-ethylenedioxythiophene (97%, EDOT), and Potassium Bromide (KBr) were obtained from Wako Pure Chemicals Co., Ltd. Phenyl amine (95%, $PhNH_2$), pyrrole (98%) were obtained from Sigma aldrich.

3-2-2. Electropolymerization test

A small amount of [DPA][HSO_4] salt powder was placed on a pre-cleaned indium tin oxide (ITO) substrate (1 × 3 cm) heated on a hotplate. When the salt was melted at around 373 K, it was spread over the substrate with a spatula, followed by heating at 373 K for 30 min. The silver paste was put on top of the substrate to make good electrical contact. Ag/AgCl and a Pt plate were used as reference and counter electrodes, respectively. Electropolymerization testing was performed in 0.1 M $HClO_4$ under two potential cycling conditions used for the evaluation of catalytic activity. One was an electrochemical cleaning process (100 cycles at a sweep rate of 50 mV s^{-1} between 0.05–1.20 V), and the other was a durability test (15,000 cycles at a sweep rate of 500 mV s^{-1} between 1.0–1.5 V). The [DPA][HSO_4] subjected to the electropolymerization test was carefully removed from the ITO electrode and was washed with ethanol before analysis of its morphology observation by SEM and chemical structure by Fourier-transform infrared spectroscopy (FTIR) spectroscopy.

3-2-3. Preparation of Pt/C catalysts using other electropolymerizable additives

Phenylammonium hydrogen sulfate ([$PhNH_3$][HSO_4]) was synthesized by simple stoichiometric neutralization of $PhNH_2$ with sulfuric acid in ethanol and subsequent solvent removal under vacuum.[67] Sputter deposition of Pt onto 0.4 ml of [DEMA][HSO_4] for 30 min

was conducted under the same conditions as shown in chapter 1. Carbon black, Vulcan® (1.5 mg) and [$PhNH_3$][HSO_4] (1.2 g, 6.3 mmol) were added to the Pt-sputtered [DEMA][HSO_4] (0.4 mL) in a vial, and it was stirred at 423 K for 20 min. Finally, the homogenized mixture was agitated at 473 K for 2 h to support Pt nanoparticles on the carbon support, washed with ultrapure water and ethanol, and dried *in vacuo* for 15 h to obtain the desired catalyst **9**.[59] Other Pt nanoparticle-supported carbon catalysts, **10**, **11**, and **12** were also prepared by a similar procedure but with 22 mg (0.22 mmol) of 3MT, 34 mg (0.51 mmol) of pyrrole, and 71 mg (0.50 mmol) of EDOT, respectively, as electropolymerizable additives instead of [$PhNH_3$][HSO_4]. For preparation of catalysts with 3MT, pyrrole, and EDOT, the heating temperature was set at 353 K, which is lower than the boiling point of charge-neutral additives. Catalyst **13** was prepared in a similar way by agitating a mixture of Pt-sputtered [$N_{1,1,1,3}$][Tf_2N] (0.4 mL) and diphenylamine (125 mg, 0.74 mmol) as electropolymerizable additives and Vulcan® at 573 K for 2 h, followed by washing several times with acetonitrile. Three types of Pt nanoparticle-supported carbon catalysts prepared using ILs and electropolymerizable additive and reported in chapter 1 and 2, Catalyst **1**, **2**, **7** and then a commercially available Pt nanoparticle catalyst, **3**, were employed for comparison.

3-2-4. Characterization and electrochemical measurements

The electrochemically treated [DPA][HSO_4] was rinsed with ethanol several times, its morphology was examined using a Hitachi S-3400N SEM under an accelerating voltage of 10 kV. The sample (0.2 mg), which was previously uniformly mixed in a mortar with well-dried KBr (40 mg), was pressed to obtain a translucent pellet for FTIR. FTIR spectroscopy was conducted on a Perkin Elmer Spectrum 100 instrument in a wavenumber range of 400–4000 cm^{-1}. The other characterization and electrochemical measurements of the Pt/C catalysts were carried out in the same method as in chapter 1.

3-3. Results and discussion

3-3-1. Electropolymerization test using [DPA][HSO_4]-coated ITO electrode

In order to explain the anomalous behavior of the Pt nanoparticle-suported carbon catalysts prepared in a PMS [DPA][HSO_4] and PIL [DEMA][HSO_4] mixture during the durability test, electrochemical examination of the [DPA][HSO_4]-coated transparent ITO electrode was conducted in a N_2-saturated 0.1 M $HClO_4$ aqueous solution. The electrode and cell used are depicted in Figure 3-1a,b. Notably, the [DPA][HSO_4] salt was firmly deposited on the ITO electrode surface without dissolution in the electrolyte solution, even when the electrochemical measurement was initiated. The electrochemical measurement was conducted under two different potential cycling conditions: first, the condition for electrochemical cleaning (0.05–1.20 V, 50 mV s^{-1}, 100 cycles); and second, the condition for the durability test (1.0–1.5 V, 500 mV s^{-1}, 15,000 cycles). Soon after immersing the [DPA][HSO_4]-coated ITO into the aqueous solution, as shown in Figure 3-1b, the transparent [DPA][HSO_4] layer changed to a white color, indicating formation of diphenylamine by the deprotonation of the $[DPA]^+$ (pK_a = 0.78).[113] Figure 3-1c shows typical cyclic voltammograms recorded at the [DPA][HSO_4]-coated ITO under the electrochemical cleaning conditions. At the first cycle, only an oxidation wave was observed at around 1.1 V. With increasing cycling number, the oxidation peak at 1.1 V became smaller, while a broad redox wave at around 0.4–0.9 V appeared and gradually increased. The white [DPA][HSO_4] layer varied to green from its edge immediately after the potential cycling was started (Figure 3-1d). This green-colored area increased upon cycling. The resulting green [DPA][HSO_4] film reversibly changed color from dark-green to yellow-green during the potential cycling. These electrochemical and electrochromic behaviors are consistent with previous reports on the electropolymerization of diphenylamine to poly(diphenylamine).[95-100] Similar behavior was also recognized under the conditions of the durability test. SEM images of the electrochemically treated [DPA][HSO_4] were very much like ones reported previously

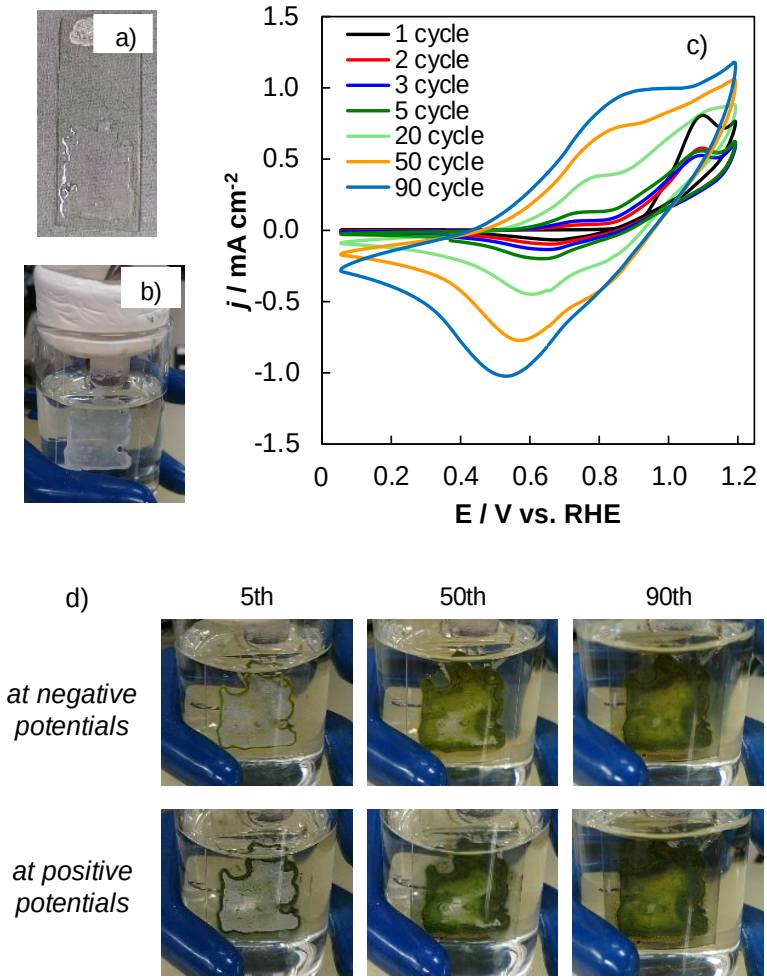

Figure 3-1. Photo images of a) a [DPA][HSO_4]-coated ITO electrode and b) an electrochemical cell for the electropolymerization test. c) Cyclic voltammograms recorded at a [DPA][HSO_4]-coated ITO electrode in a N_2-saturated 0.1 M $HClO_4$ aqueous solution during the electropolymerization test. d) Photographs of the [DPA][HSO_4]-coated ITO electrode at each cycle number during the electropolymerization test.

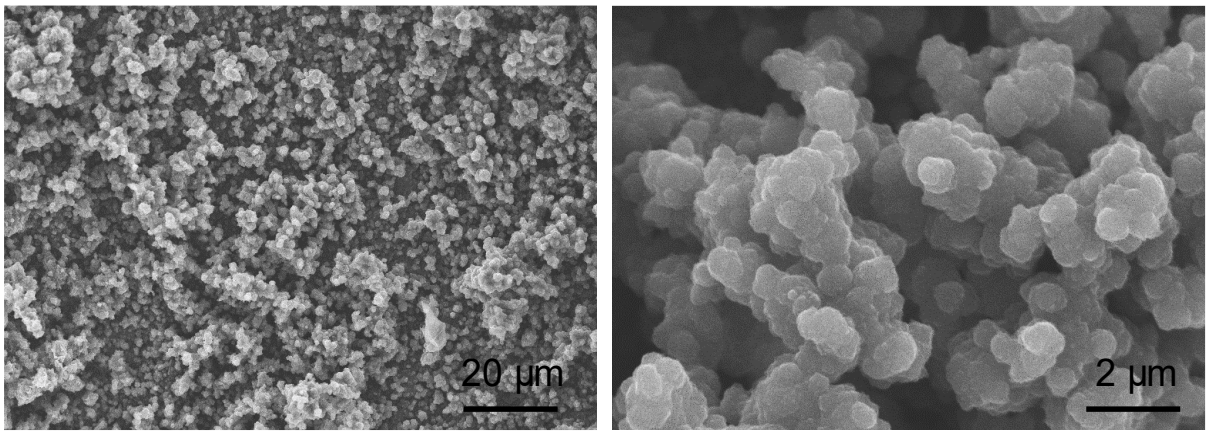

Figure 3-2. SEM images of the electropolymerized [DPA][HSO_4] after EtOH washing.

(Figure 3-2). Further investigation of the [DPA][HSO_4]-coated ITO before and after the potential cycling tests was conducted by FTIR spectroscopy. Figure 3-3 shows the FTIR spectra on the diphenylamine, as-synthesized [DPA][HSO_4], and [DPA][HSO_4] after the two potential cycling tests. The strong bands at *ca.* 815 cm^{-1}, which is assigned to *para*-coupled monomeric unit for poly(diphenylamine), appeared only at the [DPA][HSO_4] after the cycling tests,[95-100] confirming that the conductive poly(diphenylamine) was formed from [DPA][HSO_4] layer deposited on the ITO electrode in the 0.1 M $HClO_4$ aqueous solution.

Cyclic voltammetry was carried out in aqueous solution to clarify whether the elecctropolymerization of [DPA][HSO_4] occurs by the potential cycling even in the actual Pt/C catalyst prepared using [DPA][HSO_4] and in Pt nanoparticle-monodispersed PIL [DEMA][HSO_4] (catalyst **1**). Figure 3-4a shows the voltammograms obtained during electrochemical cleaning of **1**. A large oxidation current at 0.9–1.2 V was observed in the first cycle, and clear redox waves appeared at 0.7–0.8 V after the second cycle (up to the tenth cycle). This behavior is essentially consistent with that of [DPA][HSO_4]-coated ITO (Figure 3-1(c)),

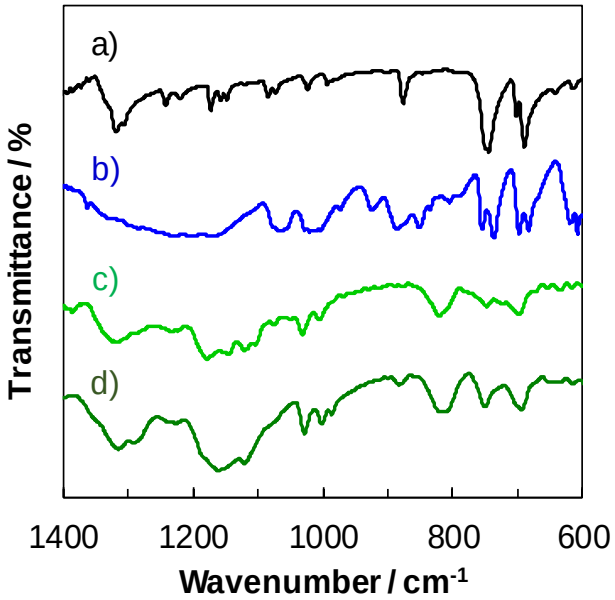

Figure 3-3. FTIR spectra of a) diphenylamine, b) as-prepared [DPA][HSO_4], and speciemen after potential cycling by c) electrochemical cleaning and d) durability test (15,000 cycles).

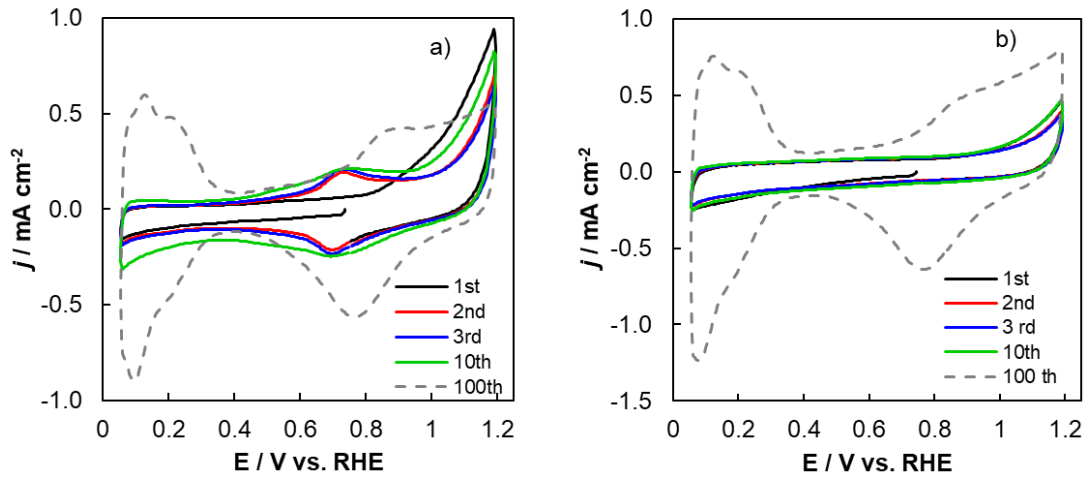

Figure 3-4. Cyclic voltammograms recorded in a N_2-saturated 0.1 M $HClO_4$ aqueous solution at a scan rate of 50 mV s^{-1} during the electrochemical cleaning of a) **1** and b) **2**.

indicating that poly(diphenylamine) was indeed formed in catalyst **1** during the electrochemical cleaning. This redox waves derived from poly(diphenylamine) formation and oxidation/reduction of the Pt surface appeared smaller and larger, respectively, after further cycling. This electrode behavior was not observed in the electrocatalyst prepared with only PIL [DEMA][HSO_4] (catalyst **2**) (Figure 3-4b). Thus, it was concluded that the high catalytic activity and durability of **1** were due to the formation of poly(diphenylamine) by the electropolymerization of [DPA][HSO_4].

3-3-2. Electrocatalytic performance and durability of the Pt/C catalysts using other electropolymerizable additives

The aforementioned electrocatalyst fabrication process was applied to other ILs and electropolymerizable additives mixtures to understand their influence on catalytic performance. [$PhNH_3$][HSO_4], 3MT, pyrrole, and EDOT were used as the electropolymerizable additives for PIL [DEMA][HSO_4] instead of [DPA][HSO_4] to synthesize the electrocatalysts **9**, **10**, **11**, and **12** respectively. However, the solubility of 3MT in [DEMA][HSO_4] was very low. In addition to those mixtures, IL [$N_{1,1,1,3}$][Tf_2N] with diphenylamine as an electropolymerizable additive

was employed for fabrication of catalyst **13**. TEM images of the five new electrocatalysts are shown in Figures 3-5. For comparison, TEM images of the previously reported Pt/C catalysts **1**, **2**, **3**, and **7**, prepared under the similar conditions reported in Chapter 2, are also shown in the Figures 2-1 in chapter 2. For **9**, **10**, and **13**, the Pt nanoparticles were homogeneously dispersed on the carbon support. Their Pt nanoparticle size distributions were analyzed; the results are shown in Figure 3-6 and Table 3. The mean particle size of Pt nanoparticles for catalyst **9**, **10**, and **13** was 2.6–3.4 nm, and the Pt loading amount was ~20–21 wt%. These values were nearly equivalent to those of the comparative catalysts. (Table 2 in chapter 2).

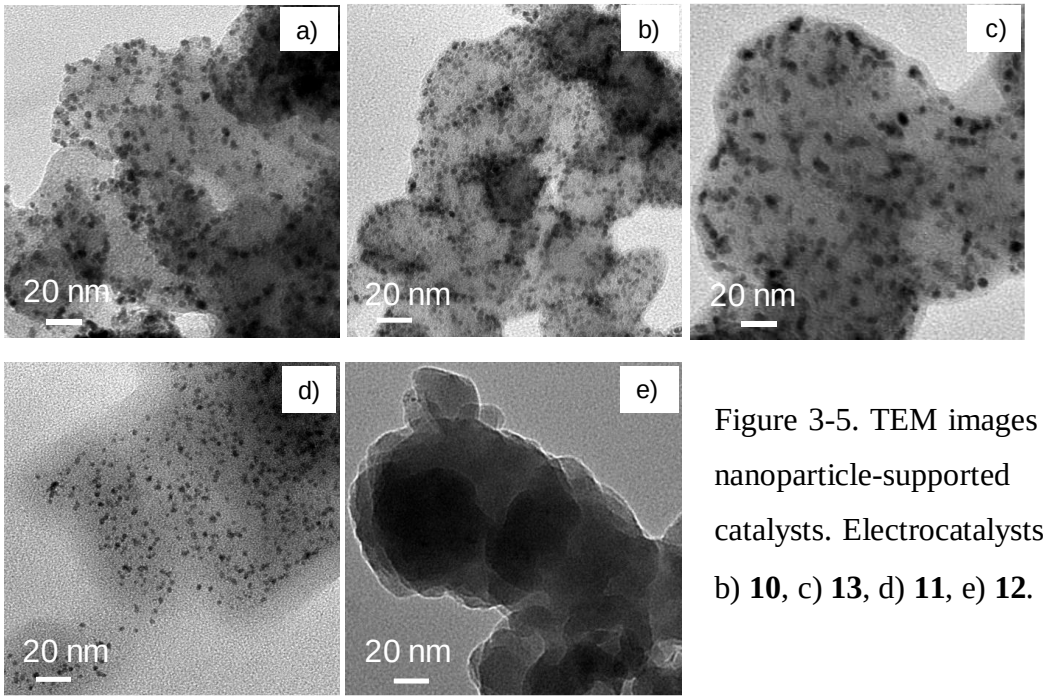

Figure 3-5. TEM images of the Pt nanoparticle-supported carbon catalysts. Electrocatalysts are a) **9**, b) **10**, c) **13**, d) **11**, e) **12**.

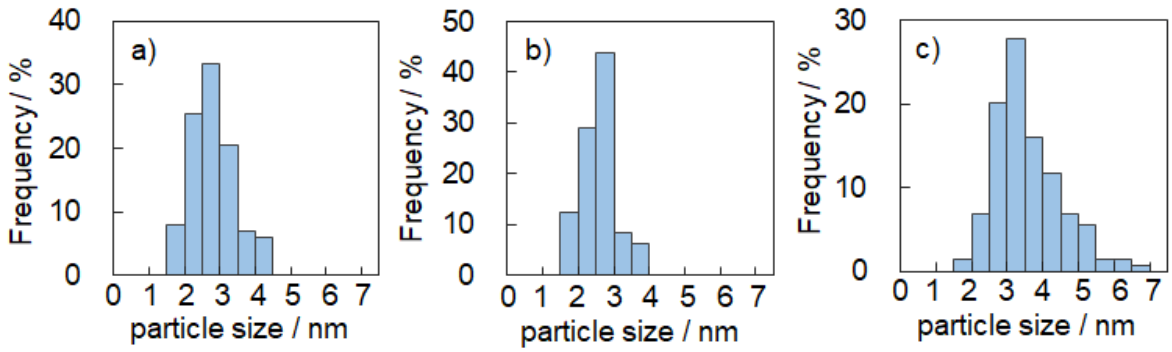

Figure 3-6. Pt size distribution of the Pt nanoparticle-supported carbon catalysts. Electrocatalysts are a) **9**, b) **10**, c) **13**.

Table 3. Summary of the Pt/C catalysts used in this chapter.

Entry	Species of ILs / additives used for catalysts	Mean particle size (nm)	Pt loading amount (wt%)	ECSA			Mass activity			$\Delta E_{1/2}$[a] (mV)
				Initial ($m^2 g^{-1}$)	After 15,000 cycles ($m^2 g^{-1}$)	Surface retention rate (%)	Initial ($A g^{-1}$)	After 15,000 cycles ($A g^{-1}$)	Catalytic activity retention rate (%)	
9	[DEMA][HSO_4] /[$PhNH_3$][HSO_4]	2.7 (0.6)[b]	20.4	40.4	39.4	97.5	341.9	465.4	136.1	- 17
10	[DEMA][HSO_4] / 3MT	2.6 (0.5)[b]	21.1	41.9	36.0	86.0	199.4	250.6	125.7	- 8
13	[$N_{1,1,1,3}$][Tf_2N] / diphenylamine	3.4 (1.0)[b]	20.2	40.6	29.7	73.3	138.1	214.6	155.4	- 23
3[c]	– / –	2.6 (0.8)[b]	26.2	51.3	15.5	30.2	273.7	173.6	63.4	41

[a] $\Delta E_{1/2}$ is the shift in the half wave potential between before and after durability test in Figure 3-11 and Figure 2-5. [b] The values show the standard deviation. [c] **3** TEC10V30E.

By contrast, the morphology of catalyst **11** and **12** clearly differed from those of other catalysts, as thermopolymerization and/or thermal decomposition of the pyrrole and EDOT readily proceeded in [DEMA][HSO_4] during the heating step in the electrocatalyst preparation process. For this reason, **11** and **12** showed no catalytic activity. Therefore, detailed electrochemical expetiments were carried out using the other three catalysts, **9**, **10** and **13**. Figure 3-7 indicates the cyclic voltammograms recorded for the three catalysts in a N_2-saturated 0.1 M $HClO_4$ aqueous solution during electrochemical cleaning. As a comparison, results for the **2** and **7** are also given in Figure 3-4b and Figure 3-7d respectively. The voltammogram recorded for **2** and **7** showed only growth of waves related to Pt, whereas the appearance and growth of other redox waves for **9**, **10**, and **13** were seen at 0.5–0.9 V in other voltammograms

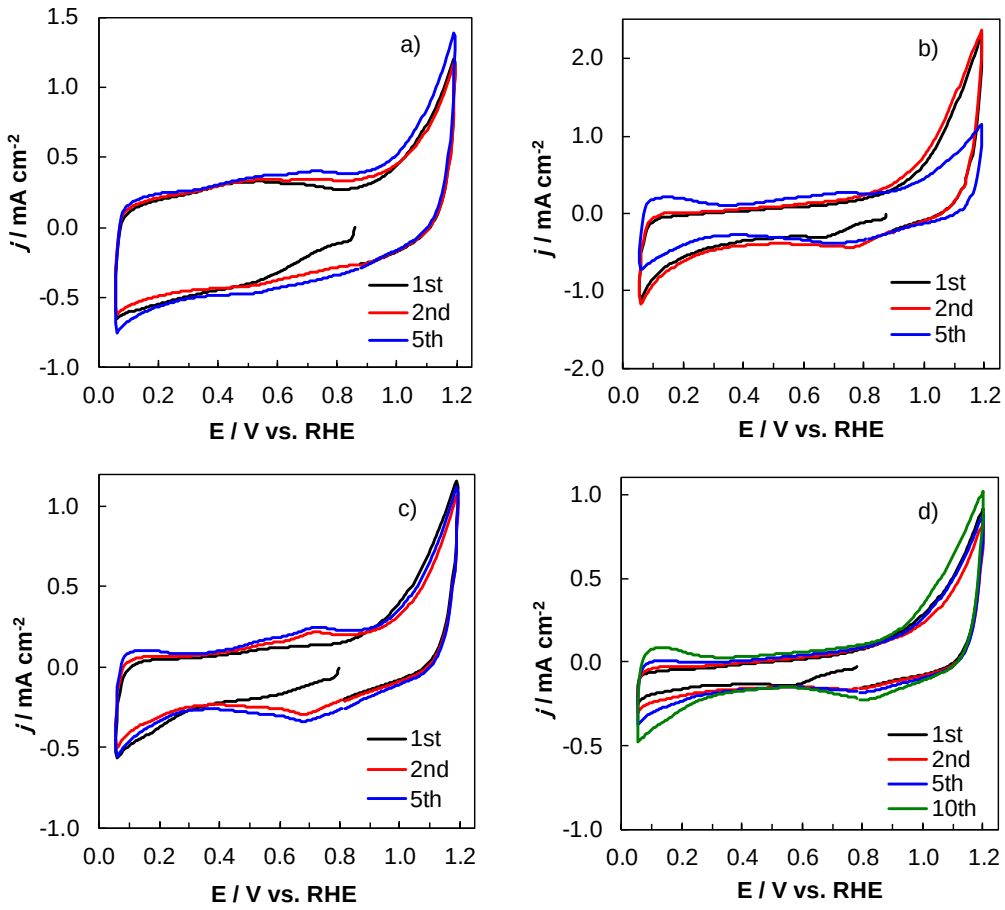

Figure 3-7. Cyclic voltammograms recorded at the different catalysts in a N_2-saturated 0.1 M $HClO_4$ aqueous solution during the electrochemical cleaning process. The catalysts were: a) **9**, b) **10**, c) **13**, and d) **7**. The scan rate was 50 mV s^{-1}.

(Figure 3-7a,b,c) similar to that for **1** shown in Figure 3-4a, suggesting electrochemical polymerization of the additives proceed in the catalyst layers. The growth of redox waves was smallest in the voltammogram of **10**, probably owing to the low solubility of 3MT in [DEMA][HSO_4].

Cyclic voltammograms obtained for **9**, **10**, and **13** in a N_2-saturated 0.1 M $HClO_4$ before and after the durability test (15,000 cycles), simulating actual fuel cell operation, are shown in Figure 3-8. Those for **1**, **2**, **3**, and **7** are also shown in Figure 2-2 of chapter 2 for comparison. In all the voltammograms, hydrogen adsorption/desorption and platinum oxidation/reduction redox waves were observed at 0.10–0.35 and 0.80–1.20 V, respectively, as observed in the

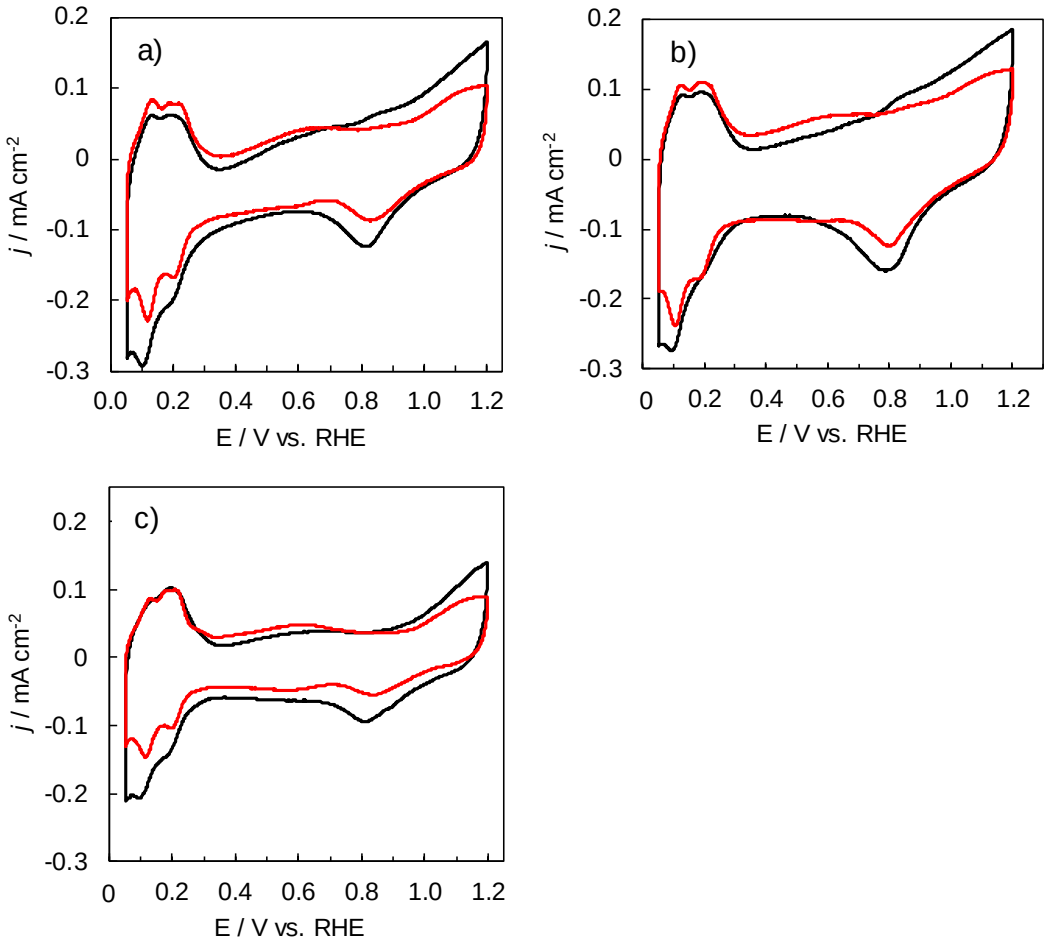

Figure 3-8. Cyclic voltammograms recorded in a N_2-saturated 0.1 M $HClO_4$ aqueous solution before (—) and after (- - -) durability test in N_2-saturated 0.1 M $HClO_4$. Electrocatalysts are a) **9**, b) **10**, c) **13**.

common Pt catalysts.[11-22,59-70] The ECSAs estimated from charge consumed by hydrogen desorption in the voltammograms before the durability test are given in Table 3. Catalysts **9**, **10**, and **13** showed initial ECSAs of 40–42 m^2 g^{-1}, similar to the values obtained for the electropolymerizable additive-free **2** and **7** (Table 2 in chapter 2), but slightly smaller than that of **3**, probably owing to a trace of the residual IL on the Pt nanoparticles meagerly preventing the adsorption of H atoms.[93,94] Figure 3-9 shows the variation in the ECSA and the surface retention rate for the ECSA on the catalyst **9**, **10**, **13**, and **3** shown in Table 3, as a function of potential cycling number, which provides important insights into the durability of the catalysts. ECSAs of all the catalysts prepared in this study increased during the first several thousand cycles, because the residual IL was removed from catalysts,[59] and gradually decreased thereafter. High surface retention rates for ECSAs (over 73%) were obtained at 15,000 cycles, although that of **3** was almost 30%. During the durability test, carbon corrosion usually proceeds *via* the oxidation of functional groups on the carbon support,[6-13] but it is inhibited by the existence of a thin IL layer between the Pt nanoparticles and the carbon support.[59] Adding the electropolymerizable additives, especially [$PhNH_3$][HSO_4] and [DPA][HSO_4], to the ILs seems to be an effective approach for further improvement. As depicted in Figure 3-10,

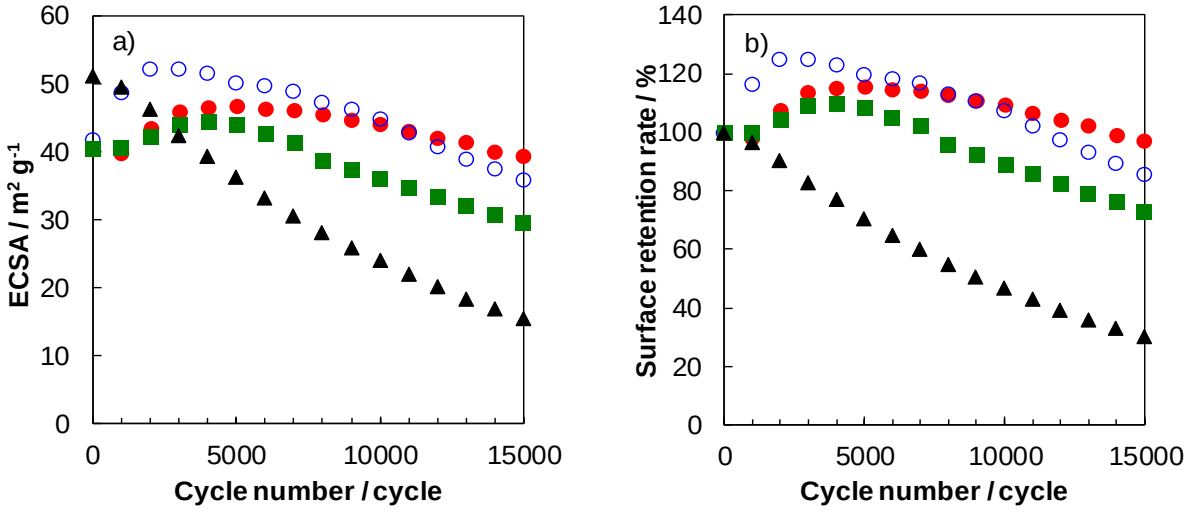

Figure 3-9. Variation in the a) ECSA and b) surface retention rate for the ECSA estimated from Figure 3-9a as a function of cycle number: ●) **9**, ○) **10**, ■) **13**, and ▲) **3**.

after the durability test, a large number of Pt nanoparticles aggregated but did not detach from the carbon support, compared with catalyst **3** shown in Figure 2-4 of Chapter 2, which was deteriorated by the carbon corrosion, causing the detachment of Pt nanoparticles.[6-13] This is in agreement with the trend of surface retention rate for the ECSA.

The ORR performances before and after the durability test were examined by RDE-LSV (Figures 3-11). The $\Delta E_{1/2}$ estimated from the obtained RDE-LSV curves are shown in the Figure 3-11. Interestingly, the $E_{1/2}$ values of the catalysts with electropolymerizable additives were positively shifted after the durability test, indicating that the catalytic activities were enhanced during the test. The mass activities before and after the durability test for all catalysts are displayed, together with their catalytic activity retention rate for the mass activity, in

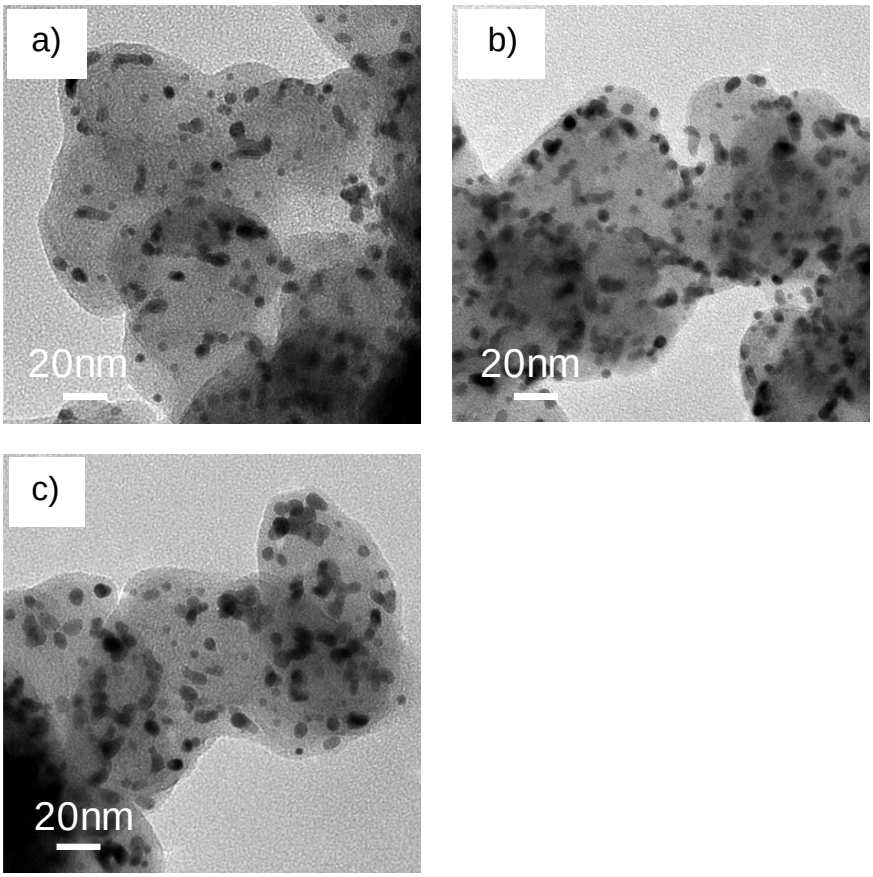

Figure 3-10. TEM images of the Pt-nanoparticle-supported carbon electrocatalysts after the durability test (15,000 cycles): a) **9**, b) **10**, c) **13**.

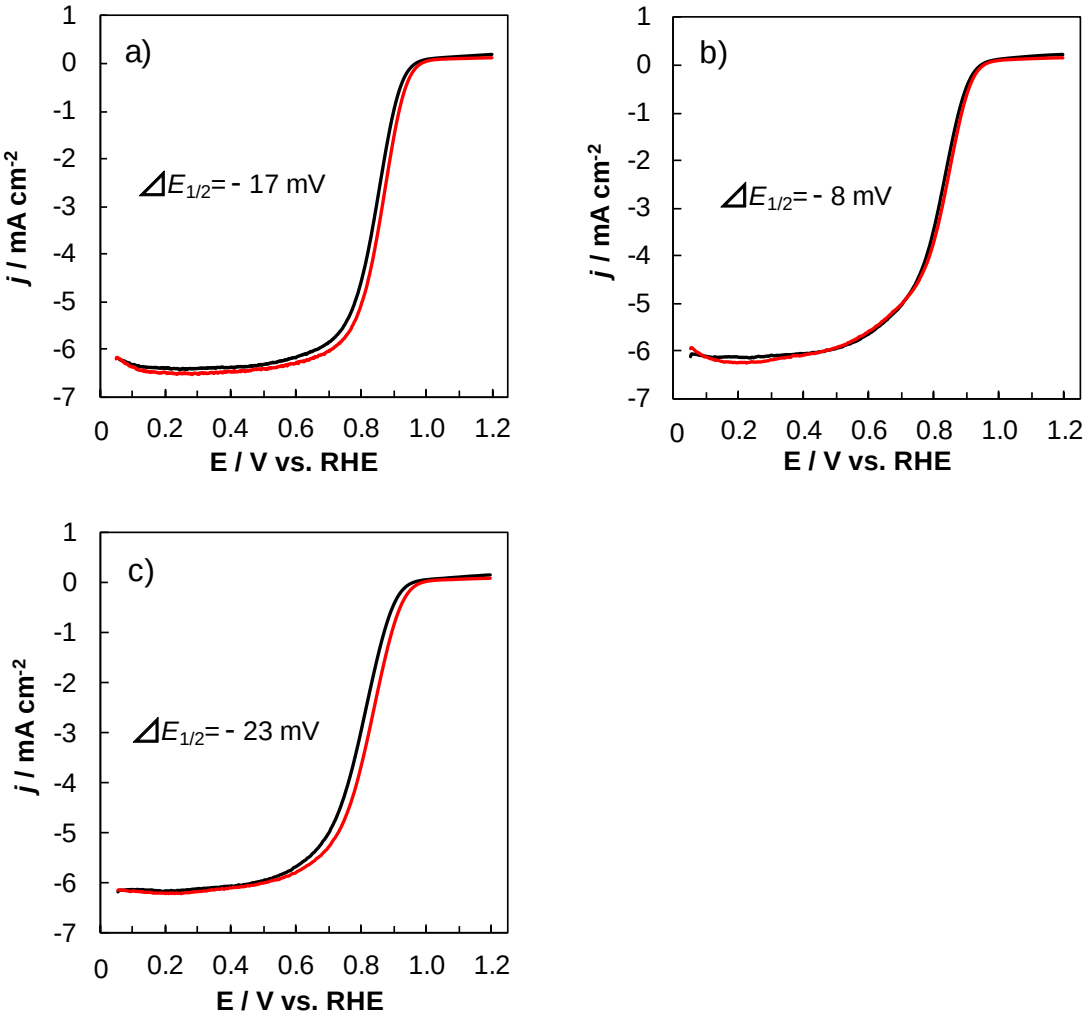

Figure 3-11. Hydrodynamic voltammograms recorded in a O_2-saturated 0.1 M $HClO_4$ aqueous solution of a) **9**, b) **10**, c) **13** electrodes before (—) and after (- - -) durability test in O_2-saturated 0.1 M $HClO_4$ at 1,600rpm.

Figure 3-12 and Table 3. All the electrocatalysts with electropolymerizable additives showed retention rates over 100 %, but rates for other electrocatalysts were unable to exceed even 90 %; for example, that of **3** was as small as 63 %. These results strongly suggest that the formation of a conductive polymer derived from electropolymerizable additives at the IL layer between Pt nanoparticles and the carbon support contributes to the enhancement of mass activity after the durability test, as well as the faborable surface retention rate estimated from the ECSA data.

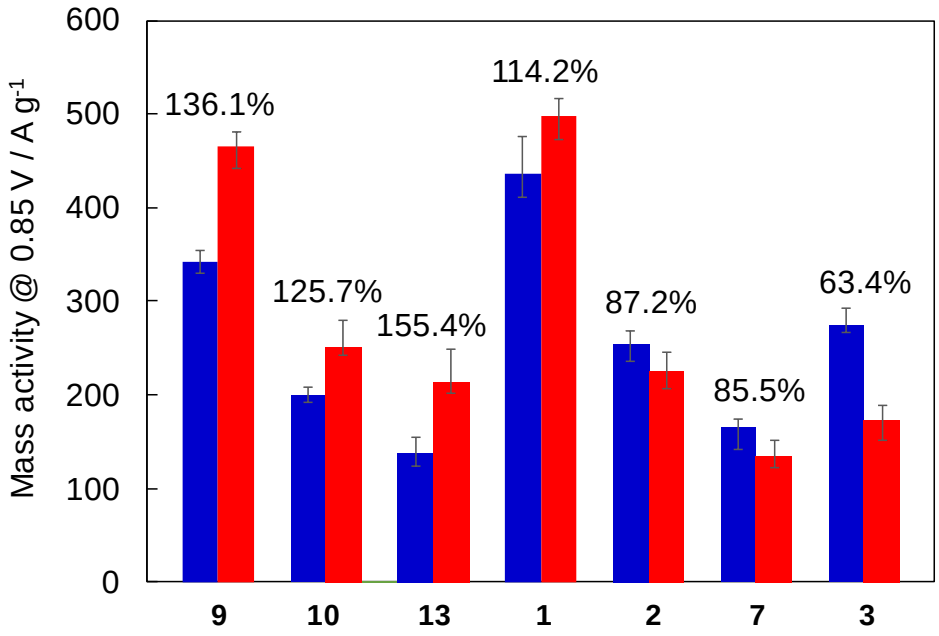

Figure 3-12. Comparison of mass activities of the four catalysts before (blue) and after (red) the durability test (15,000 cycles).

3-4. Conclusions

It was revealed that poly(diphenylamine) is formed by electropolymerization during the potential cycling of the [DPA][HSO_4]-coated ITO electrode in a N_2-saturated 0.1 M $HClO_4$ aqueous solution. Similar behavior was also observed in case of the electrocatalyst prepared using [DPA][HSO_4], suggesting that the increase in the mass activity observed at the electrocatalyst after the durability test was due to the formation of conductive poly(diphenylamine) at the IL layer between Pt nanoparticles and the carbon support. Similarly, addition of other electropolymerizable additives, [$PhNH_3$][HSO_4], 3MT, and diphenylamine, to the Pt nanoparticl-dispersed ILs enhanced the catalytic performance. This finding has important implications for designing novel functional ORR electrocatalysts. Further improvement of the electrocatalysts prepared by the approach established in this research will be achieved through more elaborate selection of electropolymerizable additives.

Summary

In this thesis, the improvement of electrocatalytic performance by the effective utilizing the function of PMS were investigated. The effect of PMS on the electrocatalytic performance of Pt/C catalyst and the hypothesis for the mechanism of the electrocatalytic performance improvement by adding PMS were discussed in each chapter of this thesis. The main results and conclusions obtained in this study are summarized as follows:

In chapter 1, the effect of PMS on electrocatalytic performance for the heated Pt/C catalyst was described. It was found that [DPA][HSO_4] which showed high carbonaceous residue yield during carbonization greatly contributed to the enhanced specific activity of Pt/C catalyst because the efficiently carbonized [DPA][HSO_4] by the heating at 1273 K reduced the charge-transfer resistance between Pt nanoparticles and carbon support, and sufficient encapsulation of Pt nanoparticles supported on the carbon support enhanced a long-term stability of the heated Pt/C catalyst.

In chapter 2, the effect of PMS on the electrocatalytic performance for the non-heated Pt/C catalyst was described. The non-heated Pt/C catalyst prepared using [DPA][HSO_4] showed surprising behavior of remarkably higher mass activity than commercially available Pt/C catalyst and the increased mass activity after durability test. The hypothesis was proposed that this improvement behavior was caused by the reduced charge-transfer resistance between Pt nanoparticles and carbon support due to the conductive polymer, poly(diphenylamine), formed through electropolymerization of [DPA][HSO_4].

In Chapter 3, verification of the hypothesis to improve electrocatalytic performance by using [DPA][HSO_4] proposed in chapter 2 was discussed. The formation of poly(diphenylamine) by the electropolymerizing [DPA][HSO_4] was confirmed because the obtained [DPA][HSO_4] through electropolymerization test showed similar electrochemical and electrochromic behaviors to poly(diphenylamine) formed by electropolymerization in acidic solution as previously reported. The Pt/C catalysts prepared by using [$PhNH_3$][HSO_4], 3MT, and diphenylamine as electropolymerizable additive also exhibited similar catalytic behavior to the case of [DPA][HSO_4], and the above hypothesis was verified.

List of Publications

1. Pt-nanoparticle-supported carbon electrocatalysts functionalized with a protic ionic liquid and organic salt

   Reiko Izumi, Yu Yao, Tetsuya Tsuda, Tsukasa Torimoto and Susumu Kuwabata

   Advanced Materials Interface, **2018**, *5*, 1701123. (Inside front cover)

2. Platinum nanoparticle-supported electrocatalysts functionalized by carbonization of a protic ionic liquid and organic salt

   Reiko Izumi, Yu Yao, Tetsuya Tsuda, Tsukasa Torimoto and Susumu Kuwabata

   ACS Appl. Energy Mater., **2018**, *1*, 3030-3034.

3. Oxygen reduction electrocatalysts sophisticated by Pt nanoparticle-dispersed ionic liquids with electropolymerizable additives

   Reiko Izumi, Yu Yao, Tetsuya Tsuda, Tsukasa Torimoto and Susumu Kuwabata

   J. Mater. Chem. A, **2018**, *6*, 11853–11862.

References

[1] V. Mehta, J. S. Cooper, *J. Power Sources* **2003**, *114*, 32–53.

[2] S. Litster, G. McLean, *J. Power Sources* **2004**, *130*, 61–76.

[3] R. Borup, J. Meyers, B. Pivovar, Y. S. Kim, R. Mukundan, N. Garland, D. Myers, M. Wilson, F. Garzon, D. Wood, P. Zelenay, K. More, K. Stroh, T. Zawodzinski, J. Boncella, J. E. McGrath, M. Inaba, K. Miyatake, M. Hori, K. Ota, Z. Ogumi, S. Miyata, A. Nishikata, Z. Siroma, Y. Uchimoto, K. Yasuda, K. Kimijima and N. Iwashita, *Chem. Rev*. **2007**, *107*, 3904–3951.

[4] Y. Wang, K. S. Chen, J. Mishler, S. C. Cho and X. C. Adroher, *Applied Energy*, **2011**, *88*, 981–1107.

[5] M. K. Debe, *Nature*, **2012**, *486*, 43–51.

[6] Y. Shao, G. Yin and Y. Gao, *J. Power Sources* **2007**, *171*, 558–566.

[7] T. Ioroi, T. Akita, M. Asahi, S. Yamazaki, Z. Siroma, N. Fujiwara and K. Yasuda, *J. Power Sources* **2013**, *223*, 183–188.

[8] A. P. Young, V. Colbow, D. Harvey, E. Rogers and S. Wessel, *J. Electrochem. Soc*. **2013**, *160*, F381–F388.

[9] Y. Yu, H. Li, H. Wang, X.-Z. Yuan, G. Wang and M. Pan, *J. Power Sources* **2012**, *205*, 10–23.

[10] X. Zhao, A. Hayashi, Z. Noda, K. Kimijima, I. Yagi and K. Sasaki, *Electrochim. Acta* **2013**, *97*, 33–41.

[11] X. Yu and S. Ye, *J. Power Sources*, **2007**, *172*, 145–154.

[12] J. Willsau, J. Heitbaum, *J. Electroanal. Chem. Interfacial Electrochem.* **1984**, *161*, 93–101.

[13] L. M. Roen, C. H. Paik and T. D. Jarvi, *Electrochem. Solid-State Lett.* **2004**, *7*, A19–A22.

[14] Z. Siroma, K. Ishii, K. Yasuda, Y. Miyazaki, M. Inaba and A. Tasaka**,** *Electrochem. Commun.* **2005**, *7*, 1153–1156.

[15] M. R. Berber, T. Fujigaya, K. Sasaki, and N. Nakashima, *Sci. Rep.* **2013**, *3*, 1764

[16] Y. Liang and H. Dai, *J. Am. Chem. Soc.*, **2012**, *134*, 15849–15854.

[17] S. Chen, Z. Wei and P. Shen, *Chem. Commun.*, **2011**, *47*, 10984–10986.

[18] S. Guo and S. Sun, *J. Am. Chem. Soc.* **2012**, *134*, 2492–2495.

[19] Y. Li, Y. Li, E. Zhu, T. McLouth, C.-Y.Chiu, X. Huang, and Y. Huang, *J. Am. Chem. Soc.* **2012**, *134*, 12326–12329.

[20] D. Higgins, P. Zamani, A, Yu and Z, Chen, *Energy Environ. Sci.* **2016**, *9*, 357–390.

[21] S. Takenaka, H. Miyamoto, Y. Utsunomiya, H. Matsune, and M. Kishida, *J. Phys. Chem. C* **2014**, *118*, 774–783.

[22] X. Xie, Y. Xue, L. Li, S. Chen, Y. Nie, W. Ding and Z. Wei, *Nanoscale* **2014**, *6*, 11035–11040.

[23] Y. Liu and W. E. Mustain, *J. Am. Chem. Soc.* **2013**, *135*, 530–533.

[24] Y. J. Wang, D. P. Wilkinson, and J. Zhang, *Chem. Rev.* **2011**, *111*, 7625–7651.

[25] Y. Shao, J. Liu, Y. Wang and Y. Lin, *J. Mater. Chem.* **2009**, *19*, 46–50.

[26] J. Zhang, K. Sasaki, E. Sutter and R. R. Adzic, *Science*, **2007**, *315*, 220–222.

[27] Y. Nie, S. Chen and Z. Wei, *Chem. Commun.*, **2014**, *50*, 15431–15434.

[28] M. Galinski, A. Lewandowski and I. Stepniak, *Electrochim. Acta* **2006**, *51*, 5567–5580.

[29] V. I. Pârvulescu, C. Hardacre, *Chem. Rev.* **2007**, *107*, 2615–2665.

[30] N. V. Plechkova, K. R. Seddon, *Chem. Soc. Rev.* **2008**, *37*, 123–150.

[31] P. Hapiot, C. Lagrost, *Chem. Rev.* **2008**, *108*, 2238–2264.

[32] F. Endres, A. P. Abbott, D. R. MacFarlane, *Electrodeposition from Ionic Liquids*, Wiley-VCH, Weinheim, **2008**.

[33] M. Armand, F. Endres, D. R. MacFarlane, H. Ohno and B. Scrosati, *Nat. Mater.* **2009**, *8*, 621–629.

[34] Z. Ma, J. Yu and S. Dai, *Adv. Mater.* **2010**, *22*, 261–285.

[35] H. Wang, G. Gurau and R. D. Rogers, *Chem. Soc. Rev.* **2012**, *41*, 1519–1537.

[36] X. Sun, H. Luo, S. Dai, *Chem. Rev.* **2012**, *112*, 2100–2128.

[37] E. F. Smith, I. J. V. Garcia, D. Briggs, P. Licence, *Chem. Commun.* **2005**, 5633–5635.

[38] S. Kuwabata, A. Kongkanand, D. Oyamatsu, T. Torimoto, *Chem. Lett.* **2006**, *35*, 600–601.

[39] S. Arimoto, H. Kageyama, T. Torimoto, S. Kuwabata, *Electrochem. Commun.* **2008**, *10*, 1901–1904.

[40] S. Arimoto, M. Sugimura, H. Kageyama, T. Torimoto and S. Kuwabata, *Electrochim. Acta* **2008**, *53*, 6228–6234.

[41] T. Torimoto, K. Okazaki, T. Kiyama, K. Hirahara, N. Tanaka and S. Kuwabata, *Appl. Phys. Lett.* **2006**, *89*, 243117.

[42] S. Kuwabata, T. Tsuda and T. Torimoto, *J. Phys. Chem. Lett.* **2010**, 3177–3188.

[43] T. Torimoto, T. Tsuda, K. Okazaki, S. Kuwabata, *Adv. Mater.* **2010**, *22*, 1196–1221.

[44] K. Okazaki, T. Kiyama, K. Hirahara, N. Tanaka, S. Kuwabata and T. Torimoto, *Chem. Commun.* **2008**, 691–693.

[45] O. P. Khatri, K. Adachi, K. Murase, K. Okazaki, T. Torimoto, N. Tanaka, S. Kuwabata and H. Sugimura, *Langmuir* **2008**, *24*, 7785–7792.

[46] K. Okazaki, T. Kiyama, T. Suzuki, S. Kuwabata and T. Torimoto, *Chem. Lett.* **2009**, *38*, 330–331.

[47] T. Suzuki, K. Okazaki, T. Kiyama, S. Kuwabata and T. Torimoto, *Electrochemistry* **2009**, 636–638.

[48] T. Tsuda, T. Kurihara, Y. Hoshino, T. Kiyama, K. Okazaki and T. Torimoto, S. Kuwabata, *Electrochemistry* **2009**, *77*, 693–695.

[49] T. Suzuki, K. Okazaki, S. Suzuki, T. Shibayama, S. Kuwabata and T. Torimoto, *Chem. Mater.* **2010**, *22*, 5209-5215.

[50] T. Suzuki, S. Suzuki, Y. Tomita, K. Okazaki, T. Shibayama, S. Kuwabata and T. Torimoto, *Chem. Lett.* **2010**, *39*, 1072–1074.

[51] Y. Oda, K. Hirano, K. Yoshii, S. Kuwabata, T. Torimoto and M. Miura, *Chem. Lett.* **2010**, *39*, 1069–1071.

[52] S. Suzuki, Y. Ohta, T. Kurimoto, S. Kuwabata and T. Torimoto, *Phys. Chem. Chem. Phys.* **2011**, *13*, 13585–13593.

[53] S. Suzuki, T. Suzuki, Y. Tomita, M. Hirano, K. Okazaki, S. Kuwabata, T. Torimoto, *CrystEngComm* **2012**, *14*, 4922–4926.

[54] M. Hirano, K. Enokida, K. Okazaki, S. Kuwabata, H. Yoshida, T. Torimoto, *Phys. Chem. Chem. Phys.* **2013**, *15*, 7286–7294.

[55] Y. Hatakeyama, M. Okamoto, T. Torimoto, S. Kuwabata and K. Nishikawa, *J. Phys. Chem. C* **2009**, *113*, 3917–3922.

[56] T. Tsuda, K. Yoshii, T. Torimoto and S. Kuwabata, *J. Power Sources* **2010**, *195*, 5980–5985.

[57] K. Yoshii, T. Tsuda, T. Arimura, A. Imanishi, T. Torimoto and S. Kuwabata, *RSC Adv*. **2012**, *2*, 8262–8264.

[58] T. Torimoto, Y. Ohta, K. Enokida, D. Sugioka, T. Kameyama, T. Yamamoto, T. Shibayama, K. Yoshii, T. Tsuda and S. Kuwabata, *J. Mater. Chem. A* **2015**, *3*, 6177–6186.

[59] K. Yoshii, K. Yamaji, T. Tsuda, R. Izumi, T. Torimoto and S. Kuwabata, *J. Mater. Chem. A* **2016**, *4*, 12152–12157.

[60] M. Antonietti, D. Kuang, B. Smarsly, Y. Zhou, *Angew. Chem. Int. Ed.* **2004**, *43*,4988–4992.

[61] P. Migowski and J. Dupont, *Chem. Eur. J.* **2007**, *13*, 32–39.

[62] C. Vollmer and C. Janiak, *Coord. Chem. Rev.* **2011**, *255*, 2039–2057.

[63] K. L. Luska and A. Moores, *ChemCatChem* **2012**, *4*, 1534–1546.

[64] H. Wender, P. Migowski, A. F. Feil, S. R. Teixeira and J. Dupont, *Coord. Chem. Rev.* **2013**, *257*, 2468–2483.

[65] A. Noda, M. A. B. H. Susan, K. Kudo, S. Mitsushima, K. Hayamizu and M. Watanabe, *J. Phys. Chem. B* **2003**, *107*, 4024–4033.

[66] S.-Y. Lee, A. Ogawa, M. Kanno, H. Nakamoto, T. Yasuda and M. Watanabe, *J. Am. Chem. Soc.* **2010**, *132*, 9764–9773.

[67] S. Zang, M. S. Miran, A. Ikoma, K. Dokko and M. Watanabe, *J. Am. Chem. Soc*. **2014**, *136*, 1690–1695.

[68] S. Zang, K. Dokko and M. Watanabe, *Chem. Mater.* **2014**, *26*, 2915–2926.

[69] W. Xu and C. A. Angell, *SCIENCE* **2003**, *302*, 422–425.

[70] L. Shi, M. Zhao, L. Zheng, *Colloids and Surfaces A* **2011**, *392*, 305–312.

[71] C. R. L.Barron and N. J. Wagner, *Langmuir* **2012**, *28*, 12722−12730.

[72] Bose, S., Armstrong, D. W., Petrich, J. W., *J. Phys. Chem. B* **2010**, *114*, 8221−8227.

[73] N. Byrne, B. Rodoni, F. Constable, S. Varghesea and J. H. Davis, *Phys. Chem. Chem. Phys.*, **2012**, *14*, 10119–10121.

[74] T. L. Greaves and C. J. Drummond, *Chem. Rev.* **2015**, *115*, 11379−11448.

[75] K. Yamamoto, D. M. Kolb, R. Kötz, G. Lehmpfuhl, *J. Electroanal. Chem. Interfacial Electrochem.* **1979**, *96*, 233–239.

[76] Fuel Cell Commercialization Conference of Japan (FCCJ), Proposals of the development targets, research and development challenges and evaluations methods concerning PEFCs, URL: http://www.fccj.jp/pdf/23_01_kt.pdf

[77] A. Iiyama, K. Shinohara, S. Iguchi and A. Daimaru, *Handbook of Fuel Cells-Fundamentals, Technology, and Application*, John Wiley & Sons, West Sussex, UK, 2009.

[78] K. H. Kangasniemi, D. A. Condit, and T. D. Jarvi, *J. Electrochem. Soc.*, **2004**, *151*, E125.

[79] C. Chen, Y. Kang, Z. Huo, Z. Zhu, W. Huang, H. L. Xin, J. D. Snyder, D. Li, J. A. Herron, M. Mavrikakis, M. Chi, K. L. More, Y. Li, N. M. Markovic, G.A. Somorjai, P. Yang and V. R. Stamenkovic, *Science* **2014**, *343*, 1339–1343.

[80] L. Zhang, L. T. Roling, X. Wang, M. Vara, M. Chi, J. Liu, S.-I. Choi, J. Park, J. A. Herron, Z. Xie, M. Mavrikakis and Y. Xia, *Science* **2015**, *349*, 412–416.

[81] V. R. Stamenkovic, B. S. Mun, M. Arenz, K. J. J. Mayrhofer, C. A. Lucas, G. Wang, P. N. Ross and N. M. Markovic, *Nat. Mater.* **2007**, *6*, 241–247.

[82] C. Wang and V. Stamenkovic, *J. Am. Chem. Soc.* **2011**, *133*, 14396–14403.

[83] L. Gan, M. Heggen, R. O'Malley, B. Theobald and P. Strasser, *Nano Lett.* **2013**, *13*, 1131–1138.

[84] X. Huang, Z. Zhao, L. Cao, Y. Chen, E. Zhu, Z. Lin, M. Li, A. Yan, A. Zetti, Y.M. Wang, X. Duan, T. Mueller and Y. Huang, *Science* **2015**, *348*, 1230–1234.

[85] X. Zhao, S. Chen, Z. Fang, J. Ding, W. Sang, Y. Wang, J. Zhao, Z. Peng and J. Zeng, *J. Am. Chem. Soc*. **2015**, *137*, 2804–2807.

[86] C. Wang, H. Daimon, T. Onodera, T. Koda and S. Sun, *Angew. Chem., Int. Ed.* **2008**, *47*, 3588–3591.

[87] T. Yu, Y. Kim, H. Zhang and Y. Xia, *Angew. Chem. Int. Ed.* **2011**, *50*, 2773–2777.

[88] J. Snyder, T. Fujita, M. W. Chen and J. Erlebacher, *Nat. Mater*. **2010**, *9*, 904–907.

[89] D. Strmcnik, M. E. Escribano, K. Kodama, V. R. Stamenkovic, A. Cuesta and N.M. Markovic´, *Nat. Chem.* **2010**, *2*, 880–885.

[90] K. Miyabayashi, H. Nishihara and M. Miyake, Langmuir. **2014**, *30*, 2936–2942.

[91] T. Tsuda and C. L. Hussey, in *Modern Aspects of Electrochemistry Vol. 45*, ; (Ed.: R. E. White). **2009**, springer Science+Bussiness Media: New York, p. 63.

[92] H. A. Gasteiger, S. S. Kocha, B. Sompalli and F. T. Wagner, *Appl. Catal. B* Env., **2005**, *56*, 9–35.

[93] M. Sobota, M. Happel, M. Amende, N. Paape, P. Wasserscheid, M. Laurin and J. Libuda, *Adv. Mater.* **2011**, *23*, 2617–2621.

[94] J. Arras, E. Paki, C. Roth, J. Radnik, M. Lucas and P. Claus, *J. Phys. Chem. C* **2010**, *114*, 10520–10526.

[95] N. Comisso, S. Daolio, G. Mengoli, R. Salmaso, S. Zecchin and G. Zotti, *J. Electroanal. Chem. Interfacial Electrochem.* **1988**, *255*, 97–110.

[96] A. Bagheri, M. E. Nateghi and A. Massoumi, *Synth. Met.* **1998**, *97*, 85–89.

[97] C.-Y. Chung, T.-C. Wen and A. Gopalan, *Elecrochim. Acta* **2001**, *47*, 423–431.

[98] U. Hayat, P. Bartlett and G. H. Dodd, *J.* Electroanal. *Chem.* **1987**, *220*, 287–294.

[99] J. Guay and Ld H. Dao. *J. Electroanal. Chem.* 1**989**, *274*, 135–142.

[100] H. Yang and A. J. Bard, *J. Electroanal. Chem.* **1991**, *306,* 87–109.

[101] E. Frackowiak and F. Beguin, *Carbon*, **2001**, *39*, 937–950.

[102] J. L. Bredas, R. Silbey, D. S. Boudreaux and R. R. Chance, *J. Am. Chem. SOC.* **1983**, *105*, 6555–6559.

[103] A. Rudge, J. Davey, I. Raistrick and S. Gottesfeld, *J. Power Sources* **1994**, *47*, 89–107.

[104] E. M. Genis, A. Boyle, M. Lapkowsky and C. Tsintavis, *Synthetic Metals* **1990**, *36,* 139–182.

[105] S. Bhadra, D.Khastgir, N. K. Singha, J. H. Lee, *Progress Polymer Science* **2009**, *34,* 783–810.

[106] J.C. Chiang and A. G. Macdiarmid, *Synthetic Metals*, **1986**, *13*, 193–205.

[107] A.F. Diaz and J.A. Longa, *J. Electroanal. Chem.* **1980**, *111*, 111–114.

[108] M.R. Gandhi, P. Murray, G.M. Spinks and G.G. Wallace, *Synthetic Metals* **1995**, *73*, 247–256.

[109] S. Geetha, Chepuri R.K. Rao, M. Vijayan and D.C. Trivedi, *Anal. Chim. Acta* **2006**, *568*, 119–125.

[110] M. Leclerc and K. Faid, *Adv. Mater.* **1997**, *9*, 1087–1094.

[111] R. K. Kline, M. D. McGhee, E. N. Kadnikova, J. Liu, J.M. Frechet, *Adv. Mater.* **2003**, *15*, 1519–1522.

[112] Y. Kim, S. Cook, S. M. Tuladhar, S. A. Coulis, J. Nelson, J. R. Durrant, D. C. Bradley, M. Gilrd, I. Mcculloch, C. S. Ha and M. Ree, *Nat. Mater.*, **2006**, *5*, 197–203.

[113] D. Dolman, R. Stewart, *Can. J. Chem.*, **1967**, *45*, 903–910.

Acknowledgement

First of all, the author would like to express her sincerest gratitude to Prof. Dr. Susumu Kuwabata, Department of Applied Chemistry, Graduate School of Engineering, Osaka University, for his continuous guidance, many invaluable suggestions and warm encouragement throughout this work. The author would like to thank to Prof. Dr. Nobuhito Imanaka and Prof. Dr. Takahiro Kozawa for their reviewing this thesis with helpful comments and suggestions.

The author also wishes to express her special thanks to Associate Prof. Dr. Tetsuya Tsuda for his continuous guidance, valuable suggestions, and many fruitful discussions throughout this work. The author would like to express her thanks to Assistant Prof. Dr. Taro Uematsu for his valuable comments and helpful supports. The author is deeply grateful to Cross-Appointment Associate Prof. Dr. Hajime Matsumoto, Department of Energy Environment, Research Institute of Electrochemical Energy, National Institute of Advanced Industrial Science and Technology, for his valuable discussions and warm guidance. The author acknowledges to Prof. Dr. Tsukasa Torimoto, Department of Materials Chemistry, Graduate School of Engineering, Nagoya University, for his expert comments. The author thanks secretary, Ms. Michiko Ebukuro for hearty supports. The author is indebted to Dr. Eiko Mchizuki, Dr. Kazuki Yoshii and Dr. Hiro Minamimoto for their fruitful discussions and expert comments. The author is also grateful to all member of Kuwabata laboratory for their heartfelt encouragements and friendship.

Finally, the author wishes to express her sincerest gratitude to her husband, Koji Izumi, her children, Koyuki Izumi and Junichiro Izumi, her mother, Yuko Kiyoshima, and her sister Kyoko Tokunaga for their warm encouragement, hearty supports and continuous understanding.

July 2018

Reiko Izumi